ScienceDirect

Fuel

Supports *open access*

9.1	5.578
CiteScore	Impact Factor

Articles & Issues ⌄   About ⌄   Pu   Submit your article ↗   Guide for authors ↗

About the journal

Aims and scope   Editorial board   Abstracting and indexing

Principal Editors

Zuohua Huang

Xi'an Jiaotong University School of Energy and Power Engineering, Xian, China

Regional Editor for East Asia, West Asia, South Asia (Except India, Bangladesh)

Bill Nimmo

The University of Sheffield, Sheffield, United Kingdom

Assisting J. Patrick

Eric Suuberg

Brown University, Providence, Rhode Island, United States of America

Regional Editor for North America, South America

Editors

Avinash Kumar Agarwal

Indian Institute of Technology Kanpur, Kanpur, India

Jorge Ancheyta

Mexican Petroleum Institute, Ciudad de Mexico, Mexico

Pietro Bartocci

University of Perugia, Perugia, Italy

Bioenergy, Life Cycle Assessment, Food Industry, Sustainability, Climate Change

Jillian L. Goldfarb

Cornell University Department of Biological and Environmental Engineering, Ithaca, New York, United States of America

Lamia Goual

University of Wyoming, Laramie, Wyoming, United States of America

Enhanced oil recovery, Flow assurance, Environmental remediation, Carbon capture and storage

Hao Liu

University of Nottingham, Nottingham, United Kingdom

Yasushi Sekine

Waseda University Faculty of Science and Engineering Department of Applied Chemistry Polymer
Chemistry, Shinjuku-Ku, Tokyo, Japan

Kevin Van Geem

Ghent University Department of Materials Textiles and Chemical Engineering Center for Sustainable
Chemistry Laboratory for Chemical Technology, Ghent, Belgium
steam cracking, fast pyrolysis, comprehensive 2D LC and GC, scale-up, process simulation, Computational
Fluid Dynamics, Kinetic modelling, combustion, fouling

International Editorial Board

Pavlos Aleiferis

Imperial College London, London, United Kingdom

Ben Anthony

CanmetENERGY, Ottawa, Ontario, Canada

Robert Brown

Iowa State University Bioeconomy Institute, Ames, Iowa, United States of America

Syed Sheraz Daood

University of the Punjab Institute of Energy and Environmental Engineering, Lahore, Pakistan

Erjiang Hu

Xi'an Jiaotong University School of Energy and Power Engineering, Xian, China

Mikko Hupa

Åbo Akademi University Physics, ABO, Finland

Marcis Jansons

Wayne State University, Detroit, Michigan, United States of America

Anker Degn Jensen

Technical University of Denmark Department of Chemical and Biochemical Engineering, Kgs Lyngby, Denmark

Jenny Jones

University of Leeds, Leeds, United Kingdom

Gerhard Knothe

USDA-ARS National Center for Agricultural Utilization Research, Peoria, Illinois, United States of America

Bo Leckner

Chalmers University of Technology, Gothenburg, Sweden

Chang Sik Lee

Hanyang University Division of Mechanical Engineering, Seongdong-gu, South Korea

Baoqing Li

Chinese Academy of Sciences State Key Laboratory of Coal Conversion, Taiyuan, China

Chun-Zhu Li

Curtin University, Perth, Western Australia, Australia

Wenying Li

Taiyuan University of Technology Key Laboratory of Coal Science and Technology, Taiyuan, China

Cherng-Yuan Lin

National Taiwan Ocean University, Keelung, Taiwan

Oliver C. Mullins

Schlumberger-Doll Research Ridgefield, Ridgefield, Connecticut, United States of America

John Patrick

University of Nottingham, Nottingham, United Kingdom

Constantine D. Rakopoulos

National Metsovian Polytechnic, Zografos, Greece

Harold H. Schobert

Schobert International LLC, Jordan, Minnesota, United States of America

Mohammad Nahid Siddiqui

King Fahd University of Petroleum & Minerals, Al Dhahran, Saudi Arabia

Juan Tascon

Spanish Scientific Research Council, Oviedo, Spain

Mark Thomas

Newcastle University, Newcastle Upon Tyne, United Kingdom

Bianca Maria Vaglieco

Institute of Engines National Research Council, Napoli, Italy

Stanislav V. Vassilev

Bulgarian Academy of Sciences, Sofia, Bulgaria

Alan Williams

University of Leeds, Leeds, United Kingdom

Dongke Zhang

The University of Western Australia Centre for Energy, Crawley, Western Australia, Australia

All members of the Editorial Board have identified their affiliated institutions or organizations, along with the corresponding country or geographic region. Elsevier remains neutral with regard to any jurisdictional claims.

ISSN: 0016-2361

Copyright © 2021 Elsevier Ltd. All rights reserved

ELSEVIER (https://w
ww.elsevi
er.com)
ELSEVIER

Home (https://www.elsevier.com/) > Journals (https://www.elsevier.com/catalog?producttype…
> Fuel (https://www.journals.elsevier.com:443/fuel)

(/fuel
/rss)

(http (//twi
://w tter.c
ww.f om/
aceb elsev
ook. ieren
com/ ergy)
elsev
ieren
ergy)

✕

We recently added gender diversity
metrics to this journal homepage.
You can find it below Journal
Metrics on the left hand side.

We are interested in your feedback
on this feature.

Any answers are anonymous and
cannot be used to identify you.

(https://www.sciencedirect
.com/science/journal/001
62361)

ISSN: 0016-2361

Fuel

The Science and Technology of Fuel and Energy

Publishing options: Open Access   (https://www.elsevier.com/journals/fuel/0016-2361/open-access-options)
   Subscription   (https://www.elsevier.com/journals/fuel/0016-2361/open-access-options)

Principal Editors: Zuohua Huang (https://www.journals.elsevier.com:443/fuel/editorial-
board/zuohua-huang), Bill Nimmo (https://www.journals.elsevier.com:443/fuel/editorial-
board/bill-nimmo), Eric Suuberg (https://www.journals.elsevier.com:443/fuel/editorial-
board/eric-suuberg)

> View Editorial Board (https://www.journals.elsevier.com:443/fuel/editorial-board)

> **CiteScore: 9.1** ⓘ   **Impact Factor: 5.578** ⓘ

Article Publishing Charge: USD 3660 excl. taxes ⓘ

Submit Your Paper (https://www.editorialmanager.com/JFUE/default.aspx)

Supports Open Access (https://www.elsevier.com/journals/fuel/0016-2361/open-access-
options)

Feedback

View Articles (https://www.sciencedirect.com/science/journal/00162361)

ELSEVIER
(https://w
ww.elsevi
Guide for Authors
er.com)
ELSEVIER

$\bigcirc$ SEARCH $\equiv$ MENU

$\vee$

Abstracting/ Indexing (http://www.elsevier.com/journals/fuel/0016-2361/abstracting-indexing)

Track Your Paper $\vee$

Order Journal $\vee$

Journal Metrics

> CiteScore: **9.1** ⓘ

Impact Factor: **5.578** ⓘ

5-Year Impact Factor: **5.776** ⓘ

Source Normalized Impact per Paper (SNIP): **2.138** ⓘ

> View More on Journal Insights

Published research articles ⓘ

	Open Access	Subscription
2020	74	2538
2019	26	2019
2018	44	1960
2017	32	1378
2016	15	1310

✕

We recently added gender diversity metrics to this journal homepage. You can find it below Journal Metrics on the left hand side.

We are interested in your feedback on this feature.

Any answers are anonymous and cannot be used to identify you.

Take the survey

United Nations Sustainable Development Goals

The journal contributes to SDGs

(https://sdgresources.relx.com/)

RELX
SDG Resource Centre

Feedback

ELSEVIER

SEARCH   MENU

Gender Diversity distribution of the Editors ⓘ

- 8% woman
- 92% man
- 0% non-binary or gender diverse
- 0% prefer not to disclose

Benchmark Gender Diversity distribution across Energy & Fuel portfolio Editors ⓘ

- 17% woman
- 83% man
- 0% non-binary or gender diverse
- 0% prefer not to disclose

Read more (https://www.elsevier.com/connect/topics/gender-and-diversity) about Elsevier on the topic of diversity &.

Access Elsevier's most recent global gender report (https://www.elsevier.com/research-intelligence/resource-library/gender-report-2020?dgcid=_EC_Connect)

Your Research Data

⟩ Share your research data (https://www.elsevier.com/authors/author-resources/research-data)

⟩ Data in Brief co-submission (https://www.journals.elsevier.com/data-in-brief/about-data-in-brief/data-in-brief-co-submission)

⟩ MethodsX co-submission (https://www.journals.elsevier.com/methodsx/about-methodsx/methodsx-co-submission)

We recently added gender diversity metrics to this journal homepage. You can find it below Journal Metrics on the left hand side.

We are interested in your feedback on this feature.

Any answers are anonymous and cannot be used to identify you.

Take the survey ✕

Related Links

⟩ Researcher Academy

⟩ Author Resources (https://www.elsevier.com/authors/author-resources)

⟩ Try out personalized alert features

Related Publications

Fuel Communications (https://www.elsevier.com/locate/inca/747495)

Feedback

Research into **energy sources** remains a key issue. Over the last 90 years, *Fuel* has been the leading source of primary research work in **fuel science**. The scope is broad and includes many topics of increasing interest such as environmental aspects and pollution.

A wide variety of fuels are covered:

•…

Read more

Most Downloaded   Recent Articles   Most Cited   Open Access Articles

Methodology for the experimental measurement of vapor–liquid equilibrium distillation curves using a modified ASTM D86 setup - Open access

Alison M. Ferris | David A. Rothamer

Characteristics of hemicellulose, cellulose and lignin pyrolysis

Haiping Yang | Rong Yan | …

Determination of flash point and cetane index in diesel using distillation curves and multivariate calibration - Open access

Helga G. Aleme | Paulo J.S. Barbeira

> View All Most Downloaded Articles (https://www.journals.elsevier.com:443/fuel/most-downloaded-articles)

✕

We recently added gender diversity metrics to this journal homepage. You can find it below Journal Metrics on the left hand side.

We are interested in your feedback on this feature.

Any answers are anonymous and cannot be used to identify you.

Take the survey

Most Downloaded Articles   ⌄

Recent Articles   Feedback

ELSEVIER
ELSEVIER
(https://w
ww.elsevi
er.com/)

f 🐦 (/fuel
       /rss)
(http (//twi
://w   tter.c
www.f om/
aceb   elsev
ook.   ieren
com/   ergy/)
elsev
ieren
ergy)

Announcements (https://www.journals.elsevier.com:443/fuel/announcements)

You can play a part in locating publications relevant to each SDG
(https://www.journals.elsevier.com:443/fuel/announcements/you-can-play-a-part-in-locating-publications-relevant-to-eac)

Elsevier working with researchers like you to build an understanding of the knowledge base related to the
United Nations Sustainable Development Goals.

In support of equality, inclusion & diversity (https://www.journals.elsevier.com:443/fuel/announcements/in-
support-of-equality-inclusion-diversity)

Elsevier stands against racism and discrimination and fully supports the joint commitment for action in
inclusion and diversity in publishing.

In partnership with the communities we serve; we redouble our deep commitment to inclusion and diversity
within our editorial, author and reviewer networks.

Heliyon Partner Journal (https://www.journals.elsevier.com:443/fuel/announcements/heliyon-partner-journal-
energy)

This journal has partnered with Heliyon Energy, a dedicated section of Heliyon, an open access journal from
Cell Press that publishes scientifically accurate and valuable research in energy. Heliyon Energy aims to make
it easier for authors to share their research with a global audience quickly and easily, while benefitting from
the subject-area expertise of specialized section editors, who ensure your work is considered fairly and reaches
the right audience. Authors can quickly and easily transfer their research from a Partner Journal to Heliyon
without the need to edit, reformat, or resubmit.

Learn more

⟩ View All (https://www.journals.elsevier.com:443/fuel/announcements)

✕

We recently added gender diversity
metrics to this journal homepage.
You can find it below Journal
Metrics on the left hand side.

We are interested in your feedback
on this feature.

Any answers are anonymous and
cannot be used to identify you.

Take the survey

Call for Papers (https://www.journals.elsevier.com:443/fuel/call-for-papers)

Special Issue on "Current Progress and Advances in Data Science for Biofuel Production and Utilisation"
(https://www.journals.elsevier.com:443/fuel/call-for-papers/current-progress)

Feedback

Special Issue on Biomass to biorefineries: A circular bioeconomy prospective (https://www.journals.elsevier.com:443/fuel/call-for-papers/biomass-to-biorefineries-a-circular-bioeconomy-prospective)

Special Issue on Gas Hydrates (https://www.journals.elsevier.com:443/fuel/call-for-papers/special-issue-on-gas-hydrates)

> View All (https://www.journals.elsevier.com:443/fuel/call-for-papers)

Special Issues (https://www.journals.elsevier.com:443/fuel/special-issues)

Special issues published in Fuel.

1st International Workshop on Oxy-Fuel Combustion
Reinhold Kneer | Johannes Janicka | ...

International Mexican Congress on Chemical Reaction Engineering (IMCCRE 2016)
Jorge Ancheyta | Gilbert F. Froment | ...

International Freiberg Conference on IGCC & XtL Technologies in 2014
Yong-Wang Li | Chris Higman | ...

> View All (https://www.journals.elsevier.com:443/fuel/special-issues)

News (https://www.journals.elsevier.com:443/fuel/news)

International Women's Day 2020 Special Issue (https://www.journals.elsevier.com:443/fuel/news/international-womens-day-2020-special-issue)

FUEL welcomes new Associate Principal Editor (https://www.journals.elsevier.com:443/fuel/news/welcome-professor-prof-avinash-kumar-agarwal)

International Conference on Coal Science & Technology (ICCS&T2019) (https://www.journals.elsevier.com:443/fuel/news/iccst201)

> View All (https://www.journals.elsevier.com:443/fuel/news)

Author Testimonials (https://www.journals.elsevier.com:443/fuel/author-testimonials)

Why do authors choose to publish their research with us? (https://www.journals.elsevier.com:443/fuel/author-testimonials/testimonials-fuel)
Read our author testimonials here

✕

We recently added gender diversity metrics to this journal homepage. You can find it below Journal Metrics on the left hand side.

We are interested in your feedback on this feature.

Any answers are anonymous and cannot be used to identify you.

Take the survey

Feedback

ELSEVIER

(https://www.elsevier.com)

ELSEVIER

> View All (https://www.journals.elsevier.com:443/fuel/author-testimonials)

(https://www.elsevier.com)

Q SEARCH   ≡ MENU

Article Digests (https://www.journals.elsevier.com:443/fuel/article-digests)

Analysing the air pollution created by hybrid electric vehicles (https://www.journals.elsevier.com:443/fuel/article-digests/analysing-the-air-pollution-created-by-hybrid-electric-vehic)

Turning ocean plastics into fuel (https://www.journals.elsevier.com:443/fuel/article-digests/turning-ocean-plastics-into-fuel)

Evaluating critical fuel properties for potential gasoline and diesel biofuel blendstocks (https://www.journals.elsevier.com:443/fuel/article-digests/evaluating-critical-fuel-properties-for-potential-gasoline)

> View All (https://www.journals.elsevier.com:443/fuel/article-digests)

Latest Mendeley Data Datasets (https://www.journals.elsevier.com:443/fuel/mendeley-data)

Mendeley Data Repository is free-to-use and open access. It enables you to deposit any research data (including raw and processed data, video, code, software, algorithms, protocols, and methods) associated with your research manuscript. Your datasets will also be searchable on Mendeley Data Search, which includes nearly 11 million indexed datasets. For more information, visit Mendeley Data.

Data for: Production of bio-jet fuel range hydrocarbons from catalytic HDO of biobased difurfurilydene acetone over Ni/SiO2-ZrO2 catalysts.

redouane bachir

15 files (2021)

Data for: Volatile release from maceral concentrates of pulverised coals used for pulverized coal injection at temperatures of 1550°C

Liza Elliott

1 file (2021)

Data for: Development of a deep learning-based model for the entire production process of steam-assisted gravity drainage (SAGD)

Yuhao Zhou

1 file (2020)

> View All (https://www.journals.elsevier.com:443/fuel/mendeley-data)

PlumX Metrics (https://www.journals.elsevier.com:443/fuel/top-articles)

Feedback

Pyrolysis of hydrothermal liquefaction algal biochar for hydrogen production in a membrane reactor

(https://plu.mx/a?doi=10.1016/j.fuel.2019.11693 5&theme=plum-cits-journa ls-theme&h ideUsage =true)

Hydrotalcite supported bimetallic (Ni-Cu) catalyst: A smart choice for one-pot conversion of biomass-derived platform chemicals to hydrogenated biofuels

(https://plu.mx/a?doi=10.1016/j.fuel.2 020.118111 &theme=plum-cits-journa ls-theme&h ideUsage =true)

Combustion, performance, and emission analysis of a CI engine fueled with mustard oil biodiesel blended in diesel fuel

(https://plu.mx/a?doi=10.1016/j.fuel.2 021.12034 6&theme=plum-cits-journa ls-theme&h ideUsage =true)

> View All (https://www.journals.elsevier.com:443/fuel/top-articles)

Article Selections (https://www.journals.elsevier.com:443/fuel/article-selections)

Article Selections

Fuel Editorial Board Member Burt Davis - in Memoriam (https://www.journals.elsevier.com:443/fuel/article-selections/fuel-editorial-board-member-burt-davis-in-memoriam)

Biodiesel Fuel Performance and Emissions (https://www.journals.elsevier.com:443/fuel/article-selections/biodiesel-fuel-performance-and-emissions)

Fuel and Combustion Science in Brazil (https://www.journals.elsevier.com:443/fuel/article-selections/fuel-and-combustion-science-in-brazil)

> View All (https://www.journals.elsevier.com:443/fuel/article-selections)

✕

We recently added gender diversity metrics to this journal homepage. You can find it below Journal Metrics on the left-hand side.

We are interested in your feedback on this feature.

Any answers are anonymous and cannot be used to identify you.

Take the survey

Conferences (https://www.journals.elsevier.com:443/fuel/conferences)

3rd International Conference for Bioresource Technology for Bioenergy, Bioproducts & Environmental Sustainability (https://www.journals.elsevier.com:443/fuel/conferences/3rd-international-conference-bioresource-technology)

International Conference on Algal Biomass, Biofuels and Bioproducts (https://www.journals.elsevier.com:443/fuel/conferences/international-conference-algal-biomass-biofuels)

> View All (https://www.journals.elsevier.com:443/fuel/conferences)

Feedback

ELSEVIER
ELSEVIER (https://www.elsevi er.com)

Data Availability Section (https://www.journals.elsevier.com:443/fuel/policies-and-guidelines/data-availability-section)

> View All (https://www.journals.elsevier.com:443/fuel/policies-and-guidelines)

Fuel

Readers
View Articles
Volume/ Issue Alert
Personalized Recommendations

Authors (http://www.elsevier.com/authors/home)
Author Information Pack (https://www.elsevier.com/journals/fuel/0016-2361?generatepdf=true)
Submit Your Paper
Track Your Paper
Researcher Academy
Rights and Permissions (https://www.elsevier.com/about/policies/copyright/permissions)
Elsevier Author Services
Webshop
Support Center

Librarians (https://www.elsevier.com/librarians)
Order Journal (http://www.elsevier.com/journals/fuel/0016-2361/order-journal)
Abstracting/ Indexing (http://www.elsevier.com/journals/fuel/0016-2361/abstracting-indexing)

Editors (http://www.elsevier.com/editors/home)
Publishing Ethics Resource Kit (http://www.elsevier.com/editors/perk)
Guest Editors (https://www.elsevier.com/editors/guest-editors)
Support Center

Reviewers (http://www.elsevier.com/reviewers/home)
Reviewer Guidelines (https://www.elsevier.com/reviewers/how-to-review)
Log in as Reviewer
Reviewer Recognition (https://www.elsevier.com/reviewers/becoming-a-reviewer-how-and-why#recognizing)
Support Center

Advertisers Media Information (https://www.elsevier.com/advertisers)

Societies (http://www.elsevier.com/societies/home)

✕

We recently added gender diversity metrics to this journal homepage. You can find it below Journal Metrics on the left hand side.

We are interested in your feedback on this feature.

Any answers are anonymous and cannot be used to identify you.

Take the survey

Feedback

(https://twitter.com/ElsevierConnect) (https://www.facebook.com/ElsevierConnect) (https://www.linkedin.com/company/elsevier) (https://www.mendeley.com/groups/) RELX Group™ (http://www.reedelsevier.com/)

✕

We recently added gender diversity metrics to this journal homepage. You can find it below Journal Metrics on the left hand side.

We are interested in your feedback on this feature.

Any answers are anonymous and cannot be used to identify you.

Take the survey

Feedback

Fuel

Supports *open access*

Articles & Issues ⌄　　　　About ⌄　　　　Publish ⌄　　　🔍　　Search in this journal

Volume 89, Issue 12

Pages 3613-4062 (December 2010)

⬇ Download full issue

〈　Previous vol/issue　　　　　　　　　　　　　　　Next vol/issue 〉

Receive an update when the latest issues in this journal are published

Sign in to set up alerts

Full text access

Editorial Board

Page IFC

⬇ Download PDF

Full Papers

FEEDBACK 💬

Fuel

Supports *open access*

Articles & Issues ⌄   About ⌄   Publish ⌄   🔍   Search in this journal

Abstract

Secondary atmospheric pollutions may result from wet flue gas desulfurization (FGD) systems caused by the reduction of Hg^{2+} to Hg^0. The present study employed three agents: Na_2S, 2,4,6-trimercaptotiazine, trisodium salt nonahydrate (TMT) and sodium dithiocarbamate (DTCR) to precipitate aqueous Hg^{2+} in simulated desulfurization solutions. The effects of the precipitator's dosing quantity, the initial pH value, the reaction temperature, the concentrations of Cl^- and other metal ions (e.g. Cu^{2+} and Pb^{2+}) on Hg^{2+} removal were studied. A linear relationship was observed between Hg^{2+} removal efficiency and the increasing precipitator's doses along with initial pH. The addition of chloride and metal ions impaired the Hg^{2+} removal from solutions due to the complexation of Cl^- and Hg^{2+} as well as the chelating competition between Hg^{2+} and other metal

Research article ○ Abstract only

Ultrasonic mixing and closed microwave irradiation-assisted transesterification of soybean oil

Ming-Chien Hsiao, Chin-Chiuan Lin, Yung-Hung Chang, Lung-Chuan Chen

Pages 3618-3622

⬇ Purchase PDF   Article preview ⌃

Abstract

Abstract

The present study employed ultrasonic mixing and closed microwave irradiation to assist transesterification of soybean oil. The purpose was to obtain the optimal ultrasonic mixing and closed microwave irradiation procedure. The optimal reaction conditions including

FEEDBACK 💬

Fuel

Supports *open access*

Articles & Issues ⌄   About ⌄   Publish ⌄   🔍   Search in this journal

Concentrations and modes of occurrence of platinum group elements in the Shengli River oil shale, northern Tibet, China

Xiugen Fu, Jian Wang, Yuhong Zeng, Fuwen Tan, Jianglin He

Pages 3623-3629

⬇ Purchase PDF   Article preview ⌃

Abstract

Abstract

The Shengli River–Changshe Mountain oil shale zone, located in the North Qiangtang depression, northern Tibet plateau, represents a potentially large marine oil shale resource in China. Twenty-one samples including oil shale, micritic limestone and marl were collected from the Shengli River area to determine the contents, distribution patterns and modes of occurrence of platinum group elements (PGEs) in marine oil shale. Oil shale samples from the Shengli River area have high ash yield (61.86–67.48%) and total organic carbon content (8.02–13.67%) with low total sulfur content (0.76–1.39%) and intermediate shale oil content (3.60–16.30%). The total PGE content in oil shale samples is very low (average 1.749 ng/g), approximately half the mean value of Chinese coals, but higher than that of USA coals. PGEs in oil shale samples from the Shengli River area are

Research article ○ Abstract only

Preparation of mullite from desilication-flyash

Anran Guo, Jiachen Liu, Rui Xu, Hai Xu, Caifen Wang

Pages 3630-3636

⬇ Purchase PDF   Article preview ⌃

Abstract

FEEDBACK 💬

Fuel

Supports *open access*

Articles & Issues ⌄　　　About ⌄　　　Publish ⌄　　　🔍　Search in this journal

new description of the flyash particle and finally benefit the utilization of flyash. Lath-like mullite crystals appeared in high-iron samples and needle-like mullite crystals were observed in low-iron

Research article　○　Abstract only

Fuel consumption and emissions from a diesel power generator fuelled with castor oil and soybean biodiesel

Osmano Souza Valente, Márcio José da Silva, Vanya Márcia Duarte Pasa, Carlos Rodrigues Pereira Belchior, José Ricardo Sodré

Pages 3637-3642

⤓ Purchase PDF　　　Article preview ⌃

Abstract

biodiesel in diesel oil, and fuel blends containing 5%, 20%, and 35% of castor oil biodiesel in diesel oil were tested, varying engine load from 9.6 to 35.7 kW. Specific fuel consumption (SFC) and the exhaust concentrations of carbon dioxide (CO_2), carbon monoxide (CO), and hydrocarbons (HC) were evaluated. The engine was kept with its original settings for diesel oil operation. The results showed increased fuel consumption with higher biodiesel concentration in the fuel. Soybean biodiesel blends showed lower fuel consumption than castor biodiesel blends at a given concentration. At low and moderate loads, CO emission was increased by nearly 40% and over 80% when fuel blends containing 35% of castor oil biodiesel or soybean biodiesel were used,

respectively, in comparison with diesel oil. With the load power of 9.6 kW, the use of fuel blends containing 20% of castor oil biodiesel or soybean biodiesel increased HC emissions by 16% and

FEEDBACK 💬

Fuel

Supports *open access*

Articles & Issues ⌄   About ⌄   Publish ⌄   🔍   Search in this journal

Abstract

In this study, the Euler–Euler (E–E) and Euler–Lagrange (E–L) models designed for the same chemical mechanism of heterogeneous reactions were used to predict the performance of a typical sudden-expanding coal combustor. The results showed that the current E–E model underestimated the coal burnout rate because the particle temperature fluctuation on char combustion is not adequately considered. A comparison of the E–E and E–L simulations showed the underestimation of heterogeneous chemical reaction rates by the E–E model.

Research article ○ Abstract only

A comprehensive mathematical model for biomass gasification in a bubbling fluidized bed reactor

Priyanka Kaushal, Jalal Abedi, Nader Mahinpey
Pages 3650-3661

⤓ Purchase PDF   Article preview ⌃

Abstract

A mathematical model of biomass gasification in bubbling fluidized gasifier has been developed. It is a one-dimensional, two-phase (bubble and emulsion), two-zone (bottom dense bed and upper freeboard), steady state model. The model is based on global reaction kinetic, mass and energy balances and is capable of predicting temperature, solid hold ups and gas concentration along the reactor's major axis. The overall model has sub-models to deal with biomass pyrolysis, gasification, bed hydrodynamics, material classification and property calculation. A sub-model for tar generation and cracking is included in this study. The model is capable of dealing with wide variety of biomasses and fluidizing agents, i.e. air, oxygen, steam or a mix of these g

FEEDBACK 💬

Fuel

Supports *open access*

Articles & Issues ⌄   About ⌄   Publish ⌄   🔍   Search in this journal

⬇ Purchase PDF   Article preview ⌃

Abstract

Abstract

A fuel quality survey of biodiesel blends collected in June 2009 from 26 Michigan retail stations was performed, 8 months after the publication of ASTM D7467. Measured blend levels were not consistent in stations where pump labels indicate specific biodiesel blend levels. Fatty acid methyl ester (FAME) analyses revealed that majority of the samples are soybean oil-based (SBO) biodiesel. Full compliance with the ASTM D7467 requirements for kinematic viscosity and flash point (FP) were observed with the biodiesel blends; all but one for cetane number (CN). Barely half of the samples were able satisfy the total acid number (TAN) specification with select samples reflecting as high as 1.6 mg KOH/g. The most pressing is that only 45% were able to meet the 6 h induction period (IP) requirement; out of those that did not qualify 42% are even low blends hinting the

Research article ○ Abstract only

Study on the phosphate removal from aqueous solution using modified fly ash

Ke Xu, Tong Deng, Juntan Liu, Weigong Peng

Pages 3668-3674

⬇ Purchase PDF   Article preview ⌃

Abstract

Abstract

In this work the fly ash was modified by sulfuric acid for the removal of phosphate. It was found that modification of fly ash could significantly enhance the phosphate immobilizati

FEEDBACK 💬

Fuel

Supports *open access*

Articles & Issues ⌄   About ⌄   Publish ⌄   🔍   Search in this journal

Research article ○ Abstract only

Synthesis of biodiesel from edible, non-edible and waste cooking oils via supercritical methyl acetate transesterification

Pasquale Campanelli, Mauro Banchero, Luigi Manna

Pages 3675-3682

⤓ Purchase PDF   Article preview ⌃

Abstract

Abstract

The use of methyl acetate instead of methanol for supercritical synthesis of glycerol-free biodiesel from vegetable oils is a new process and its study is very limited in the literature. In this work, it has been tested for the first time on three edible and non-edible oils with different fatty acid composition. The process was also applied to waste oil with higher free fatty acid (FFA) content. The results demonstrate that the oil composition does not significantly influence the biodiesel yield.

The influence of temperature, pressure and molar ratio of reactants was studied. All the oils achieved complete conversion after 50 min at 345 °C, 20 MPa with methyl acetate:oil molar ratio

Research article ○ Abstract only

Determination of the reactive component of fly ashes for geopolymer production using XRF and XRD

Ross P. Williams, Arie van Riessen

Pages 3683-3692

FEEDBACK 💬

Fuel

Supports *open access*

Articles & Issues ⌄   About ⌄   Publish ⌄   🔍   Search in this journal

geopolymers made with fly ash from coal-fired power stations. The accepted method of determining the formulation of geopolymers to get the desired matrix chemistry uses the bulk composition of the feedstock materials. This formulation method is widely used in investigations using feedstock materials that almost completely react during processing. It is widely considered that amorphous components of fly ash are the reactive components in the geopolymerisation reaction. However, quantification of the amorphous components is challenging and generally

Research article   ○ Abstract only

Numerical investigation of Solid Recovered Fuels' co-firing with brown coal in large scale boilers – Evaluation of different co-combustion modes

Michalis Agraniotis, Nikos Nikolopoulos, Aris Nikolopoulos, Panagiotis Grammelis, Emmanuel Kakaras
Pages 3693-3709

⬇ Purchase PDF   Article preview ⌃

Abstract

Abstract

In the current work the co-combustion of Solid Recovered Fuels' (SRFs') with brown coal in large scale pulverised coal boilers under different operational conditions is numerically investigated. In order to overcome the difficulty of the complex, inhomogeneous nature of waste recovered fuels, SRF is modelled as a mixture of two different fractions, the biogenic and the plastic one. For each fraction different combustion mechanisms are presented, whilst for the first time the proposed combustion mechanism of the plastic fraction is incorporated in a commercial CFD code and validated against available experimental data. A 600 MW_e brown coal boiler is simulated as a reference and its operational characteristics are compared with parameterised scenarios of SRF co-

FEEDBACK 💬

Fuel

Supports *open access*

Articles & Issues ⌄   About ⌄   Publish ⌄   🔍   Search in this journal

Abstract

Abstract

The present study represents an effort to correlate the dependence of NO_x emissions on heat losses to the atmospheric environment in a CH_4/air fueled combustor. To this end, the numerical analysis was performed over a wide range of residence times, equivalence ratios and heat losses using a perfectly stirred reactor (PSR) code. The numerical results showed that the calculated NO_x concentration initially increased, reached a maximum value and then decreased with increasing residence time when the heat loss was present. The similar variation was observed in changes in the thermal NO concentration that was evaluated by only considering the reactions associated with the thermal (Zeldovich) NO mechanism. With the heat loss increased, the calculated NO_x concentration was substantially reduced for all equivalence ratios investigated. In addition, the

Research article ○ Abstract only

Sunflower biodiesel production and application in family farms in Brazil

Anderson Favero Porte, Rosana de Cassia de Souza Schneider, Jonas Alvaro Kaercher, Rodrigo Augusto Klamt, ... Wolmar Alípio Severo Filho

Pages 3718-3724

⬇ Purchase PDF   Article preview ⌃

Abstract

Abstract

There are limited options available for compact small-scale biodiesel production equipment that produces biodiesel of similar quality as that obtained from an industrial-scale production system. The aim of the present study was to evaluate equipment optimization for producing

FEEDBACK 💬

Fuel

Supports *open access*

Articles & Issues ⌄　　　About ⌄　　　Publish ⌄　　　🔍　Search in this journal

Forage turnip, sunflower, and soybean biodiesel obtained by ethanol synthesis: Production protocols and thermal behavior

C.M. Soares, L.C.V. Itavo, A.M. Dias, E.J. Arruda, … L.C.S. de Oliveira

Pages 3725-3729

⬇ Purchase PDF　　Article preview ⌃

Abstract

Abstract

In this work it is reported a detailed investigation of the effect of different production protocols based on alkaline ethanolysis on conversion yield of forage turnip, soybean, sunflower, and castor oil into the respective biodiesel. Parameters such as catalyst contents, reaction times and temperatures were evaluated. Additionally, it was also investigated the relationship between the conversion yield and the chemical composition of the fatty acids in the feedstock. Conversion yields ranging between 70% and 100% point out the viability of the production of biodiesel using ethanol. Based on thermal analysis, sequential steps of weight loss were observed indicating that biodiesel undergoes oxidative thermal decomposition with the elimination of different portions of the molecules in each step. Besides, the energies released by the samples during thermal

Research article ○ Abstract only

Tracking aromaticity changes in heavy hydrocarbon processing by monitoring changes in electrical resistivity

Clovis Bombardelli, Lívia Mari Assis, Hypolito José Kalinowski

Pages 3730-3734

⬇ Purchase PDF　　Article preview ⌃

FEEDBACK 💬

Fuel

Supports *open access*

Articles & Issues ⌄　　　About ⌄　　　Publish ⌄　　　🔍　　　Search in this journal

determine the temperature necessary for thermal cracking reactions and the kinetic parameters of heavy petroleum fractions.

Research article ○ Abstract only

Atomization and combustion of canola methyl ester biofuel spray

Jaime A. Erazo, Ramkumar Parthasarathy, Subramanyam Gollahalli

Pages 3735-3741

⬇ Purchase PDF　　　Article preview ⌃

Abstract

Abstract

The spray atomization and combustion characteristics of canola methyl ester (CME) biofuel are compared to those of petroleum based No. 2 diesel fuel in this paper. The spray flame was contained in an optically accessible combustor which was operated at atmospheric pressure with a co-flow of heated air. Fuel was delivered through a swirl-type air-blast atomizer with an injector orifice diameter of 300 μm. A two-component phase Doppler particle analyzer was used to measure the spray droplet size, axial velocity, and radial velocity distributions. Radial and axial distributions of NO, CO, CO_2 and O_2 concentrations were also obtained. Axial and radial distributions of flame temperature were recorded with a Pt–Pt/13%Rh (type R) thermocouple. The volumetric flow rates of fuel, atomization air and co-flow air were kept constant for both fuels. The droplet Sauter mean

Research article ○ Abstract only

Thermal analysis of a diesel engine operating with diesel–biodiesel blends

FEEDBACK 💬

Fuel

Supports *open access*

Articles & Issues ⌄   About ⌄   Publish ⌄   🔍   Search in this journal

periodic boundary condition on the surface in contact with the combustion gases. The heat transfer coefficient at the top surface was modeled taking into account the temperature and pressure inside the combustion chamber. Such instantaneous pressure was measured using a special probe for an engine operating with several blends of diesel and biodiesel, and the temperature was obtained through a First Law analysis. The physical properties, including the cetane number were evaluated experimentally for all diesel/biodiesel blends used in this work. An elliptic scheme of numerical grid generation was used, so that the irregular shaped piston in the physical domain was transformed into a cylinder in a computational domain. The timewise

Research article ○ Abstract only

An investigation of the catalytic abatement of emissions from the combustion of diesel/bioethanol blends

Grisel Corro, Edgar Ayala, Nallely Tellez, Mario M. Bustillo Diaz
Pages 3753-3757

⤓ Purchase PDF   Article preview ⌃

Abstract

Abstract

In this study, we investigated the activity of pre-sulfated $1\%Pt–2\%Sn/\gamma–Al_2O_3$ on the catalytic abatement of the combustion emissions of three fuels: pure diesel E(0), pure bioethanol E(100) and bioethanol blended diesel containing 10% bioethanol E(10). The emissions generated, by each blend combustion, were conducted continuously to the catalyst sample. The catalytic activity was determined by following the evolution of the outflow emissions concentrations by FTIR gas spectroscopy as a function of the catalyst temperature. Results showed that the addition of

FEEDBACK 💬

Fuel

Supports *open access*

Articles & Issues ⌄   About ⌄   Publish ⌄   🔍   Search in this journal

Abstract

Abstract

A gas jet superposition model has been recently developed for computing group-hole nozzle sprays in computational fluid dynamics (CFD) simulations. The objectives of this study are: (1) to perform a systematic validation of the comprehensive spray model for group-hole nozzles using a broad range of experimental data; (2) to analyze the dynamics and physical insight of group-hole nozzle sprays based on the simulation results; and (3) to further clarify the impact of included-angle on spray/mixture properties of group-hole nozzle sprays. An updated version of the KIVA-3V Release 2 code, which employs the Lagrangian-Drop Eulerian-Fluid (LDEF) methodology for numerical calculation of two-phase flows, was used in the simulations. Diverging group-hole nozzles with various included-angles were considered. The test conditions included non-evaporating and

Research article ○ Abstract only

Biomass direct chemical looping process: Process simulation

Fanxing Li, Liang Zeng, Liang-Shih Fan
Pages 3773-3784

⬇ Purchase PDF   Article preview ⌃

Abstract

Abstract

Biomass is a clean and renewable energy source. The efficiency for biomass conversion using conventional fuel conversion techniques, however, is constrained by the relatively low energy

FEEDBACK 💬

Fuel

Supports *open access*

Articles & Issues ⌄   About ⌄   Publish ⌄   🔍   Search in this journal

Evaluation of guindilla oil (*Guindilia trinervis* Gillies ex Hook. et Arn.) for biodiesel production

Ricardo San Martín, Teófilo de la Cerda, Adolfo Uribe, Paola Basilio, ... Marlene Gebauer

Pages 3785-3790

⬇ Purchase PDF   Article preview ⌃

Abstract
───

Abstract

Guindilla plants (*Guindilia trinervis* Gillies ex Hook. et Arn.) are small shrubs that grow wildly in the mountains of Central Chile in soils and climates not suitable for agriculture. Whole guindilla seeds contain 28–29% w/w oil. Cotyledons represent 45% w/w of the seed and contain 63–64% w/w oil. Main unsaturated fatty acids are oleic (63% w/w), linoleic (8% w/w) and gadoleinic (9.5% w/w), while main saturated fatty acids are palmitic (9.1% w/w) and stearic (3.1% w/w). The content of free fatty acids was 0.06%. Transesterification reactions yielded a biodiesel with ester content >99%; cetane number 59; oxidative stability at 110 °C, 18.9 h; kinematic viscosity at 40 °C, 4.867 mm^2/s; cold filter plugging point, CFPP + 4 °C; sulfur content 1.0 mg/kg; sulfated ash < 0.01% p/p; acid value 0.024 mg KOH/g and phosphorous content (<0.5 mg/kg). All values were within European and US

Research article ○ Abstract only

Biodiesel production by ethanolysis of mixed castor and soybean oils

Daniela da Costa Barbosa, Tatiana M. Serra, Simoni M. Plentz Meneghetti, Mario R. Meneghetti

Pages 3791-3794

⬇ Purchase PDF   Article preview ⌃

FEEDBACK 💬

Fuel

Supports *open access*

Articles & Issues ⌄   About ⌄   Publish ⌄   🔍   Search in this journal

mixture.

Research article ○ Abstract only

Modelling of an updraft fixed-bed gasifier operated with softwood pellets

C. Mandl, I. Obernberger, F. Biedermann

Pages 3795-3806

⬇ Purchase PDF   Article preview ⌃

Abstract

Abstract

This paper presents a one-dimensional steady state mathematical model for the simulation of a small scale fixed-bed gasifier. The model is based on a set of differential equations describing the entire gasification process of softwood pellets and is solved by a two step iterative method. The main features of the model are: homogeneous and heterogeneous combustion and gasification reactions, one-step global pyrolysis kinetics and drying, heat and mass transfer in the solid and gas phases as well as between phases, heat loss, particle movement and shrinkage within the bed. The pyrolysis model has been improved by partially cracking primary tar into lighter gases according to experimental data. The model is used to simulate a laboratory scale fixed-bed updraft gasifier. Good agreement is achieved between prediction and measurements for the axial temperature

Research article ○ Abstract only

Limitations of the use of cetane index for alternative compression ignition engine fuels

Noel Bezaire, Kapila Wadumesthrige, K.Y. Simon Ng, Steven O. Salley

FEEDBACK 💬

Fuel

Supports *open access*

Articles & Issues ⌄　　　About ⌄　　　Publish ⌄　　　🔍　　Search in this journal

cetane index. The best agreement among three methods was observed for ULSD, while S-8 showed the largest discrepancy. The cetane indices for S-8 were 70.2 and 67.3 calculated using D4737 and D976 respectively, while the DCN was 52.8. The addition of biodiesel to ultra low sulfur diesel (ULSD) fuel alters the chemical properties of the fuel. The derived cetane number reflected the increase in ignition quality with the addition of biodiesel while calculations for cetane index did not. The cetane indices for a commercial B20 were 45.30 and 46.70 while the DCN showed a

Research article ○ Abstract only

Investigation of the combustion of neat cottonseed oil or its neat bio-diesel in a HSDI diesel engine by experimental heat release and statistical analyses

C.D. Rakopoulos, D.C. Rakopoulos, E.G. Giakoumis, A.M. Dimaratos
Pages 3814-3826

⤓ Purchase PDF　　　Article preview ⌃

Abstract

Abstract

An experimental study is conducted to evaluate the effects of using neat cottonseed oil or its neat ME (methyl ester) bio-diesel, on the combustion behavior of a standard, high speed, direct injection (HSDI), 'Hydra' diesel engine located at the authors' laboratory. Combustion chamber and fuel injection pressure diagrams are obtained at medium and high load using a developed, high-speed, data acquisition and processing system. A heat release analysis of the experimentally obtained cylinder pressure diagrams is developed and used. Plots of histories in the combustion chamber of the heat release rate and other related parameters reveal some interesting features,

FEEDBACK 💬

Fuel

Supports *open access*

Articles & Issues ⌄   About ⌄   Publish ⌄   🔍   Search in this journal

Abstract

Abstract

The paper presents the experimental results obtained concerning performances and pollution of a diesel engine fueled with diesel–biodiesel–ethanol blends compared with diesel fuel in laboratory tests. The main properties of the researched fuels are presented within this paper, in comparison with classical diesel fuel (chemical composition, density, kinematic viscosity, cold filter plugging point, flash point). Engines' performances were evaluated by determining the brake specific fuel consumption and brake thermal efficiency. For pollution evaluation the emissions of CO, CO_2, NO_x, HC and smoke have been measured. An increasing of brake specific fuel consumption has been observed, especially at lower engines' loads, with maximum 32.4%, reducing engine brake thermal efficiency with maximum 21.7%. CO emissions decrease, especially at high loads with

Research article ○ Abstract only

Optimization of supercritical dimethyl carbonate (SCDMC) technology for the production of biodiesel and value-added glycerol carbonate

Kok Tat Tan, Keat Teong Lee, Abdul Rahman Mohamed
Pages 3833-3839

⬇ Purchase PDF   Article preview ⌃

Abstract

Abstract

FEEDBACK 💬

Fuel

Supports *open access*

Articles & Issues ⌄   About ⌄   Publish ⌄   🔍   Search in this journal

---

Research article ○ Abstract only

Emission characteristics of diesel, gas to liquid, and biodiesel-blended fuels in a diesel engine for passenger cars

Gunfeel Moon, Yonggyu Lee, Kyonam Choi, Dongsoo Jeong

Pages 3840-3846

⬇ Purchase PDF   Article preview ⌃

Abstract

out emission characteristics for alternative fuels. In this respect, an experimental study was conducted on a 2.0 L 4 cylinders turbocharged diesel engine fuelled with those alternative diesel fuels to investigate the engine-out emission characteristics under various steady-state engine operating conditions. The results revealed that noticeable decreases in THC (22–56%) and CO (16–52%) emissions for GTL–biodiesel blends were observed, whereas NOx emissions for GTL–biodiesel blends increased by a maximum of 12% compared to diesel. With regard to particle size distributions (PSDs) for GTL–biodiesel blends, the particulate matter (PM) number concentration in accumulation mode decreased, as a result of the excess oxygen content in biodiesel. Contrary to the tendency in the accumulation mode, there was a slight increase in the PM number concentration in the nucleation mode under the operating conditions wherein the exhaust gas

Research article ○ Abstract only

Effect of MEA fabrication techniques on the cell performance of Pt–Pd/C electrocatalyst for oxygen reduction in PEM fuel cell

Sarawalee Thanasilp, Mali Hunsom

Pages 3847-3852

FEEDBACK 💬

Fuel

Supports *open access*

Articles & Issues ⌄   About ⌄   Publish ⌄   🔍 Search in this journal

(PEM) fuel cell was carried out under identical conditions of Pt–Pd/C electrocatalyst loading. The results indicated that the fabrication technique had only a very slight effect on the ohmic resistance of the PEM fuel cell but it significantly affected the charge transfer resistance and open circuit voltage (OCV). The cells prepared by the CCM method, and particularly by decal transfer, exhibited a significantly higher OCV but a lower ohmic and charge transfer resistance compared with the other investigated fabrication techniques. By using cyclic voltammetry with H₂ adsorption, it was

Research article ○ Abstract only

Fly ash-supported cerium triflate as an active recyclable solid acid catalyst for Friedel–Crafts acylation reaction

Chitralekha Khatri, Deepti Jain, Ashu Rani

Pages 3853-3859

⬇ Purchase PDF   Article preview ⌃

Abstract

Abstract

An efficient solid Lewis acid, has been synthesized by loading cerium triflate (7 wt%) on the acid activated fly ash with high silica content (81%). The physico-chemical properties of synthesized fly ash-supported cerium triflate catalyst (CFT) were monitored by XRD, FT-IR spectroscopy, FT-IR spectroscopy of the ammonia adsorbed catalyst, SEM-EDAX, TEM, Flame Atomic Absorption Spectrophotometer and TG-DTA study. The increased concentration of silica surface hydroxyl groups on activated fly ash have a major influence on the loading of cerium triflate. The catalytic activity of the catalyst CFT was tested in the acylation of veratrole using acetic anhydride as the acylating agent. The proposed model structure of CFT shows that the triflate species withdraws the

FEEDBACK 💬

Fuel

Supports *open access*

Articles & Issues ⌄   About ⌄   Publish ⌄   🔍   Search in this journal

Abstract

Abstract

Previously water-in-octane nano-emulsions were prepared by mixed surfactant systems. In this paper, a series of amphiphilic graft copolymers, namely poly (higher α-olefin-*co-para*-methylstyrene)-*graft*-poly(ethylene glycol) and poly (higher α-olefin-*co*-acrylic acid)-*graft*-poly(ethylene glycol), were used as additives to enhance the stability of these nano-emulsions. Although the amphiphilic graft copolymers did not impact the average diameter of the water droplets in these emulsions to a major extent, the stability of these emulsions were enhanced significantly by the interaction between surfactants and amphiphilic graft copolymers. Amphiphilic graft copolymers' stabilizing capability depends on their chain structure and composition. In a proper range of poly(ethylene glycol) content, e.g. 6.0–34.0 wt.%, the higher the

Research article ○ Abstract only

Accelerating transesterification reaction with biodiesel as co-solvent: A case study for solid acid sulfated tin oxide catalyst

Man Kee Lam, Keat Teong Lee

Pages 3866-3870

⬇ Purchase PDF   Article preview ⌃

Abstract

Abstract

Solid acid catalysts are normally used to catalyze the transesterification of oil with high free fatty acid (FFA) to biodiesel. However, the immiscible phases of methanol-oil-catalyst in the initial

FEEDBACK 💬

Fuel

Supports *open access*

Articles & Issues ⌄   About ⌄   Publish ⌄   🔍   Search in this journal

Low boiling point organic amine-catalyzed transesterification of cottonseed oil to biodiesel with trace amount of KOH as co-catalyst

Jianfeng Yao, Lei Ji, Peiyong Sun, Lixiong Zhang, Nanping Xu

Pages 3871-3875

⬇ Purchase PDF   Article preview ⌃

Abstract

Abstract

The effect of addition of trace amount of KOH as co-catalyst on low boiling point organic amine-catalyzed transesterification for biodiesel production was investigated. Three different organic amines, tri-ethylamine, di-ethylamine and tert-butylamine, were used as catalysts, and the maximum amount of KOH that could be added to these organic amine-catalyzed systems was 367.1 mg/kg oil. Under such circumstance, KOH could be left in the resultant biodiesel and no washing was needed to remove it as the concentration of K^+ in the biodiesel met EN 14214 standards. Addition of trace amount of co-catalyst KOH with an amount of 367.1 mg/kg oil resulted in the organic amine-catalyzed transesterification under milder reaction conditions than those without addition of KOH to achieve >90% yield of methyl ester. Furthermore, side reactions

Research article   ○   Abstract only

The impact of soy-based biodiesel on PAH, nitro-PAH and oxy-PAH emissions from a passenger car operated over regulated and nonregulated driving cycles

George Karavalakis, George Deves, Georgios Fontaras, Stamoulis Stournas, ... Evangelos Bakeas

Pages 3876-3883

⬇ Purchase PDF   Article preview ⌃

FEEDBACK 💬

Fuel

Supports *open access*

Articles & Issues ∨　　　About ∨　　　Publish ∨　　　🔍　Search in this journal

PAHs, 4 nitro-PAHs and 6 oxy-PAHs were determined in the exhaust. The results obtained, showed that PAH emissions decreased with the addition of biodiesel during all driving modes. However, their nitrated and oxygenated products were found to increase with biodiesel compared to diesel fuel. The use of pure biodiesel led in some increases in PAH emissions when compared to

Research article ⭘ Abstract only

Morphological characterization of super fine pulverized coal particle. Part 2. AFM investigation of single coal particle

Jiaxun Liu, Xiumin Jiang, Xiangyong Huang, Shaohua Wu
Pages 3884-3891

⬇ Purchase PDF　　　Article preview ∧

Abstract

Abstract

Super fine pulverized coal combustion is a new pulverized coal combustion technology which has better stability, higher combustion efficiency and lower NO_x and SO_2 emission than that using conventional particle sizes. In this paper we applied fractal analysis based on power spectral density (PSD) and slit island method (SIM), three-dimensional (3D) surface roughness measurement and surface-topography observations from AFM to form a proper investigative tool which may give a relatively full picture of surface morphology of super fine pulverized coal particles for the first time. The final results indicate that both fractal dimensions calculated by SIM and PSD and roughness of coal particle size increase with the increase of the coal particle size. Besides, the grey relational analysis was used to study the degree of relative importance of the

FEEDBACK 💬

Fuel

Supports *open access*

Articles & Issues ⌄　　　About ⌄　　　Publish ⌄　　　🔍　Search in this journal

collected from the 15 coal-burning thermal power plants (TPPs) in operation by means of gamma spectrometric technique and to assess the radiological impacts from the utilization of PFA samples examined as filling and cover material in earthwork applications. Also, the annual effective doses received by workers handling PFA and members of the public living in a house near the PFA pile/landfill were estimated using methods specified in the Radiation Protection 122. The activity concentrations of ^{226}Ra, ^{232}Th and ^{40}K measured in PFA samples were tabulated for each TPP. The activity results show that Turkish PFA may have relatively high natural radioactivity content, depending on its origin reaching in the case of Kangal PFA 2720 Bq kg^{-1} of ^{226}Ra. The values of external exposure indexes (radium equivalent activity index and gamma index) calculated for PFA

Research article ◯ Abstract only

Two-stage equilibrium model applicable to the wide range of operating conditions in entrained-flow coal gasifiers

Thanh D.B. Nguyen, Young-Il Lim, Byung-Ho Song, Si-Moon Kim, … Dal-Hong Ahn
Pages 3901-3910

⬇ Purchase PDF　　　Article preview ⌃

Abstract

Abstract

A two-stage equilibrium model applicable to the wide range of operating conditions is developed to predict carbon conversion and composition of the product gas in an entrained-flow coal gasifier. The model is composed of two separate stages including char-gasification and gas-phase reaction. Carbon conversion is estimated in the first stage with solid–gas reactions, and then the product

FEEDBACK 💬

Fuel

Supports *open access*

Articles & Issues ⌄   About ⌄   Publish ⌄   🔍   Search in this journal

T.G. Bridgeman, J.M. Jones, A. Williams, D.J. Waldron

Pages 3911-3918

⬇ Purchase PDF   Article preview ⌃

Abstract

Abstract

The process of torrefaction alters the physical properties of biomass, reducing its fibrous tenacious nature. This could allow increased rates of co-milling and therefore co-firing in coal fired power stations, which in turn would enable a reduction in the amount of coal used and an increase in the use of sustainable fuels, without the need for additional plant. This paper presents an experimental investigation of the pulverisation behaviour of two torrefied energy crops, namely: willow and Miscanthus. A multifactorial method approach was adopted to investigate the three process parameters of temperature, residence time and particle size, producing fuels treated using four different torrefaction conditions. The untreated and torrefied fuels were subjected to standard fuel analysis techniques including ultimate analysis, proximate analysis and calorific value

Research article ○ Abstract only

Effect of injection and ignition timings on performance and emissions from a spark-ignition engine fueled with methanol

Jun Li, Chang-Ming Gong, Yan Su, Hui-Li Dou, Xun-Jun Liu

Pages 3919-3925

⬇ Purchase PDF   Article preview ⌃

Abstract

FEEDBACK 💬

Fuel

Supports *open access*

Articles & Issues ⌄　　About ⌄　　Publish ⌄　　　🔍　Search in this journal

maximum in-cylinder pressure, the maximum heat release rate, and higher thermal efficiency compared to the case of non-optimized injection and ignition timings. For methanol engine, the

Research article　○　Abstract only

A direct numerical simulation study of coherent oscillation effects of swirling flows

Nan Gui, JianRen Fan, Kefa Cen, Song Chen
Pages 3926-3933

⬇ Purchase PDF　　　Article preview ⌃

Abstract

Abstract

In this study, we carried out a direct numerical simulation of swirling jets to investigate the temporal characteristics of coherent structures related to the vortex breakdown. The type of coherent motion of oscillation, as a temporal characteristic of vortex breakdown, is observed through the analysis of correlation functions. It indicates that the vortex breakdown is accompanied with the resonance of fluctuations of flow velocity, pressure, vortices and etc. Moreover, it is found that the coherent oscillation occurs only for the swirling flows with a high level of swirl (larger than the critical value) when the bubble vortex breakdown takes place, and only at relatively moderate Reynolds numbers transiting from laminar to turbulence.

Research article　○　Abstract only

The effect of hydrothermal dewatering of Pontianak tropical peat on organics in wastewater and gaseous products

FEEDBACK 💬

Fuel

Supports *open access*

Articles & Issues ⌄   About ⌄   Publish ⌄   🔍   Search in this journal

Pontianak, West Kalimantan Indonesia, on the amounts of organic compounds released into wastewater and gaseous products. Hydrothermal upgrading and dewatering of the peat was carried out in a batch-type autoclave reactor at temperatures between 150 and 380 °C at a maximum pressure of 25.1 MPa for 30 min. It was found that the extent of decomposition of organics during hydrothermal dewatering depended on temperature increase.

Wastewater from hydrothermal dewatering was found to contain organic carbon (TOC) ranging from 800 ppm at low temperatures, to 7504 ppm at high temperatures. A number of sugars and

Research article ○ Abstract only

Study of kinetics of co-pyrolysis of coal and waste LDPE blends under argon atmosphere

Sumedha Sharma, Aloke K. Ghoshal

Pages 3943-3951

⬇ Purchase PDF   Article preview ⌃

Abstract

Abstract

Co-pyrolysis of coal with waste plastic is increasingly being looked upon as a potential technique to counter the present day challenges in energy and waste management by harnessing the multiple benefits associated with the same. In the present work, the kinetics of co-pyrolysis of waste LDPE carried out with coal of *Ledo* origin from the coalfields of Assam (India) has been studied. A thermo-gravimetric (TG) study of the co-pyrolysis has been carried out taking waste LDPE-coal mixtures in ratios of 3:1, 1:1, and 1:3 by weight and at five varying heating rates from 5 to 25 K min^{-1} with a 5 K increment. Experiments were also carried out for the individual components

FEEDBACK 💬

Fuel

Supports *open access*

Articles & Issues ⌄   About ⌄   Publish ⌄   🔍   Search in this journal

Abstract

gasoline/ethanol and gasoline–surrogate/ethanol mixtures containing 10%, 20% and 30% of alcohol in volume. A hybrid burner specially designed to stabilize different liquid fuels flames with identical hydrodynamic conditions has been used. Spatially resolved measurements of soot volume fraction and of soot precursors concentration have been carried out by coupling Laser-Induced Incandescence (LII) at 1064 nm and Laser-Induced Fluorescence (LIF) at 532 nm. Significant reductions of the concentrations of soot and soot precursors have been observed when adding ethanol to gasoline. A similar behaviour has been obtained with a gasoline–surrogate which has been found to reproduce well the sooting propensity of the unleaded gasoline used in this work. The analysis of the correlation existing between the peak soot volume fraction measured in flames and the Threshold Soot Index (TSI) of the different mixtures tested in this work revealed that the

Research article ⭘ Abstract only

Synthesis and component confirmation of biodiesel from palm oil and dimethyl carbonate catalyzed by immobilized-lipase in solvent-free system

Liping Zhang, Shuzhen Sun, Zhong Xin, Boyang Sheng, Qun Liu

Pages 3960-3965

⬇ Purchase PDF   Article preview ⌃

Abstract

Abstract

The transesterification of palm oil and dimethyl carbonate (DMC) for preparing biodiesel has been carried out at the catalysis of immobilized-lipase in solvent-free system. The compo

FEEDBACK 💬

Fuel

Supports *open access*

Articles & Issues ⌄   About ⌄   Publish ⌄   🔍   Search in this journal

---

Research article ◯ Abstract only

Surface modification of high calcium fly ash for its application in oil spill clean up

O.K. Karakasi, A. Moutsatsou

Pages 3966-3970

⬇ Purchase PDF   Article preview ⌃

Abstract

(HCO)). Two HCFA samples, a Ca-rich one (AD) and a Si-rich one (M), have been examined, so as to investigate the role of HCFA composition in its behaviour. The addition of HCFA to an oil spill results in the formation of a semi-solid oil–HCFA phase, allowing the quite total removal of oil from the water surface. HCFA's oil sorption capacity in dry environment after 24 h is 0.7–0.9 g oil/g HCFA for AD and 0.5–0.6 g oil/g HCFA for M. HCFA's behaviour, when added to an oil spill, necessitates the amelioration of its floating ability and affinity for oil and to this direction its hydrothermal treatment in an aqueous solution of sodium oleate (SO) under several conditions (time, temperature, HCFA:SO mass ratio, SO solution concentration, solution:HCFA ratio) has been applied. The treatment of the calcareous HCFA (AD) at 25 °C at a mass ratio HCFA:SO = 1:0.004 results in the formation of a cohesive semi-solid oil–HCFA phase, allowing the total removal of oil

---

Research article ◯ Abstract only

Hydrodynemics of a cocurrent upflow liquid–liquid reciprocating plate reactor for homogeneously base-catalyzed methanolysis of vegetable oils

Ivica S. Stamenković, Ivana B. Banković-Ilić, Predrag B. Jovanić, Vlada B. Veljković, Dejan U. Skala

Pages 3971-3984

⬇ Purchase PDF   Article preview ⌃

FEEDBACK 💬

Fuel

Supports *open access*

Articles & Issues ⌄   About ⌄   Publish ⌄   🔍   Search in this journal

important reaction operating conditions on the pressure fluctuation at the reactor bottom, the power consumption, the dispersed phase holdup, the Sauter-mean drop diameter and the specific interfacial area. The power consumption under batch, single- and two-phase flow was proved to depend on the vibration intensity. The Sauter-mean drop diameter was found to depend on the

Research article ○ Abstract only

Effect of temperature on the performance of microbial fuel cells

A. Larrosa-Guerrero, K. Scott, I.M. Head, F. Mateo, ... C. Godinez
Pages 3985-3994

⬇ Purchase PDF   Article preview ⌃

Abstract

Abstract

Single and double chamber microbial fuel cells (MFCs) were tested in batch mode at different temperatures ranging from 4 to 35 °C; results were analysed in terms of efficiency in soluble organic matter removal and capability of energy generation. Brewery wastewater diluted in domestic wastewater (initial soluble chemical oxygen demand of 1200 and 492 mg L^{-1} of volatile suspended solids) was the source of carbon and inoculum for the experiments. Control reactors (sealed container with support for biofilm formation) as well as baseline reactors (sealed container with no support) were run in parallel to the MFCs at each temperature to assess the differences between water treatment including electrochemical processes and conventional anaerobic digestion (in the presence of a biofilm, or by planktonic cells). MFCs showed improvements

Research article ○ Abstract only

FEEDBACK 💬

Fuel

Supports *open access*

Articles & Issues ⌄   About ⌄   Publish ⌄   🔍   Search in this journal

droplets. The effects of interaction between droplets are taken into account based on the experimentally determined corrections to Nusselt and Sherwood numbers. It is pointed out that the interactions between droplets lead to noticeable reduction of their heating in the case of ethanol, 3-pentanone, n-heptane, n-decane and n-dodecane droplets, and reduction of their cooling in the case of acetone. Although the trends of experimentally observed droplet temperatures and radii are the same as predicted by the model taking into account the interaction between droplets, the actual values of the predicted droplet temperatures can differ from the observed ones by up to about 8 K, and the actual values of the predicted droplet radii can differ from the observed ones by

Research article   ○ Abstract only

Influence of porosity and surface groups on the catalytic activity of carbon materials for the microwave-assisted CO_2 reforming of CH_4

B. Fidalgo, A. Arenillas, J.A. Menéndez

Pages 4002-4007

⬇ Purchase PDF   Article preview ⌃

Abstract

Abstract

In this work, various carbon materials were studied as catalysts/microwave receptors for the CO_2 reforming of the CH_4 reaction. Carbon materials with a different textural development (metallurgical coke, activated carbons, re-activated carbon) were selected as catalysts in order to determine the role of porosity and pore size in dry reforming. Microporosity was found to be necessary for a good performance of the carbon catalysts. An activated carbon and an oxidized activated carbon were compared in order to evaluate the influence of oxygen surface

FEEDBACK 💬

Fuel

Supports *open access*

Articles & Issues ⌄   About ⌄   Publish ⌄   🔍 Search in this journal

Pages 4008-4013

⤓ Purchase PDF   Article preview ⌃

Abstract

Abstract

Conventional fossil diesel fuel and renewable diesel fuel based on hydrotreated vegetable oils (HVO) were compared regarding the oxidation characteristics of the generated soot particulate. The comparison was performed by utilizing a high-temperature oxidation tandem differential mobility analyser in which monodisperse soot aerosol was first selected and then heated in a high-temperature furnace. The particle size reduction caused by oxidation during the furnace treatment was then measured as a function of furnace temperature. The results indicate that soot oxidation is very similar between the studied fuels. This is supported by the obtained HR-TEM images and EELS-spectra which were practically indistinguishable between different fuels and engine conditions. The similar oxidation properties and surface structure between fossil and HVO-based

Research article ○ Abstract only

A comparison of injector flow and spray characteristics of biodiesel with petrodiesel

S. Som, D.E. Longman, A.I. Ramírez, S.K. Aggarwal
Pages 4014-4024

⤓ Purchase PDF   Article preview ⌃

Abstract

Abstract

FEEDBACK 💬

Fuel

Supports *open access*

Articles & Issues ⌄   About ⌄   Publish ⌄   🔍   Search in this journal

Research article ○ Abstract only

Experimental investigation of an industrial scale black liquor gasifier. 1. The effect of reactor operation parameters on product gas composition

Per Carlsson, Henrik Wiinikka, Magnus Marklund, Carola Grönberg, ... Rikard Gebart

Pages 4025-4034

⬇ Purchase PDF   Article preview ⌃

Abstract

Abstract

A novel technology to mitigate the climate changes and improve energy security is Pressurized Entrained flow High Temperature Black Liquor Gasification (PEHT-BLG) in combination with an efficient fuel synthesis using the resulting syngas. In order to optimise the technology for use in a pulp and paper mill based biorefinery, it is of great importance to understand how the operational parameters of the gasifier affect the product gas composition. The present paper is based on experiments where gas samples were withdrawn from the hot part of a 3 MW entrained flow pressurized black liquor gasifier of semi industrial scale using a high temperature gas sampling system. Specifically, the influence of process conditions on product gas composition (CO_2, CO, H_2, CH_4, H_2S, and COS) were examined by systematically varying the operational parameters: system

Research article ○ Abstract only

Optimization of pretreatment reaction for methyl ester production from chicken fat

Ertan Alptekin, Mustafa Canakci

Pages 4035-4039

FEEDBACK 💬

Fuel

Supports *open access*

Articles & Issues ⌄   About ⌄   Publish ⌄   🔍   Search in this journal

offal and trims after rendering process. However, chicken fats often contain significant amounts of FFA which cannot be converted to biodiesel using an alkaline catalyst due to the formation of soap. Therefore, the FFA level should be reduced to desired level (below 1%) by using acid catalyst before transesterification. For this aim, sulfuric, hydrochloric and sulfamic (amidosulfonic) acids were used for pretreatment reactions and the variables affecting the FFA level including alcohol molar ratio, acid catalyst amount and reaction time were investigated by using the chicken fat with

Research article ○ Abstract only

Ash deposition during the co-firing of bituminous coal with pine sawdust and olive stones in a laboratory furnace

P. Abreu, C. Casaca, M. Costa

Pages 4040-4048

⬇ Purchase PDF   Article preview ⌃

Abstract

Abstract

This article describes an experimental study on ash deposition during the co-firing of bituminous coal with pine sawdust and olive stones in a laboratory furnace. The main objective of this study was to relate the ash deposit rates with the type of biomass burned and its thermal percentage in the blend. The thermal percentage of biomass in the blend was varied between 10% and 50% for both sawdust and olive stones. For comparison purposes, tests have also been performed using only coal or only biomass. During the tests, deposits were collected with the aid of an air-cooled deposition probe placed far from the flame region, where the mean gas temperature was around 640 °C. A number of deposit samples were subsequently analyzed on a scanning electron

FEEDBACK 💬

Fuel

Supports *open access*

Articles & Issues ⌄   About ⌄   Publish ⌄   🔍   Search in this journal

⬇ Purchase PDF   Article preview ⌃

Abstract

Abstract

In the mezcal industry, the xerophyte A*gave salmiana* is used to produce mezcal, and neither the plant nor its residues have been studied before as an alternative source of fuel. Bagasse and wasted fibers samples from alcoholic beverage production were collected in order to find out their properties as fuel. Another sample consists in pyrolyzed bagasse at 450 °C to produce carbon. DSC results revealed differences in the heat of combustion values, where pyrolyzed bagasse (19.36 MJ/kg) had a higher value than bagasse (9.55 MJ/kg) or the fiber (8.4 MJ/kg). SEM images showed the morphological changes in the fibers after their processing. TGA analysis showed the presence of different alcohols impregnated on the bagasse, which allows for an increase in heat of combustion. With these preliminary results it can be seen that it is possible to use the byproducts generated by

Short communication ○ Abstract only

Drag coefficient of Solid Recovered Fuels (SRF)

Gregory Dunnu, Jörg Maier, Uwe Schnell, Günter Scheffknecht

Pages 4053-4057

⬇ Purchase PDF   Article preview ⌃

Abstract

Abstract

FEEDBACK 💬

Fuel

Supports *open access*

Articles & Issues ∨　　　　About ∨　　　Publish ∨　　　🔍　　Search in this journal

Letters to the Editor

Correspondence ⚪ No access

Photographic records of volatile release in the rapid heating of Victorian brown coals

J.C. Jones

Page 4058

⤓ Purchase PDF

Correspondence ⚪ No access

The composition of syngas from coal-biomass gasification

J.C. Jones

Page 4059

⤓ Purchase PDF

Correspondence ⚪ No access

Thermocouple signals from a fluidised bed reactor

J.C. Jones

Page 4060

⤓ Purchase PDF

Correspondence ⚪ No access

The possible importance of solubility parameter in carbon dioxide sequestration in coal mines

J.C. Jones

FEEDBACK 💬

Fuel

Supports *open access*

Articles & Issues ⌄   About ⌄   Publish ⌄   🔍   Search in this journal

ISSN: 0016-2361

ⓡ RELX™

ELSEVIER

FEEDBACK 💬

ScienceDirect

Fuel

Fuel

Supports *open access*

9.1
CiteScore

5.578
Impact Factor

Submit your article   Guide for Authors

Latest issue   All issues   • • •

Search in this journal

Volume 89, Issue 12

Pages 3613-4062 (December 2010)

⬇ Download full issue

‹ **Previous vol/issue**   **Next vol/issue** ›

Receive an update when the latest issues in this journal are published

Sign in to set up alerts

Full text access

Editorial Board

Page IFC

⤓ Download PDF

Full Papers

Research article ○ Abstract only

Enhanced Hg^{2+} removal and Hg^0 re-emission control from wet fuel gas desulfurization liquors with additives

Tingmei Tang, Jiang Xu, Rongjie Lu, Jingjing Wo, Xinhua Xu

Pages 3613-3617

⤓ Purchase PDF   Article preview ⌃

Abstract

---

precipitate aqueous Hg^{2+} in simulated desulfurization solutions. The effects of the precipitator's dosing quantity, the initial pH value, the reaction temperature, the concentrations of Cl^- and other metal ions (e.g. Cu^{2+} and Pb^{2+}) on Hg^{2+} removal were studied. A linear relationship was observed between Hg^{2+} removal efficiency and the increasing precipitator's doses along with initial pH. The addition of chloride and metal ions impaired the Hg^{2+} removal from solutions due to the complexation of Cl^- and Hg^{2+} as well as the chelating competition between Hg^{2+} and other metal ions. Based on a comprehensive comparison of the treatment effects, DTCR was found to be the most effective precipitating agent. Moreover, all the precipitating agents were potent enough to inhibit Hg^{2+} reduction as well as Hg^0 re-emission from FGD liquors. More than 90% Hg^{2+} was captured by precipitating agents while Hg^{2+} reduction efficiency decreased from 54% to just less

---

Research article ○ Abstract only

Ultrasonic mixing and closed microwave irradiation-assisted transesterification of soybean oil

Ming-Chien Hsiao, Chin-Chiuan Lin, Yung-Hung Chang, Lung-Chuan Chen

Pages 3618-3622

⤓ Purchase PDF   Article preview ⌃

Abstract

Abstract

The present study employed ultrasonic mixing and closed microwave irradiation to assist transesterification of soybean oil. The purpose was to obtain the optimal ultrasonic mixing and closed microwave irradiation procedure. The optimal reaction conditions including amount of catalyst used, reaction temperature and methanol/oil molar ratio were also investigated to achieve the highest possible conversion rate of biodiesel. Results showed that the optimal procedure involved 1-min ultrasonic mixing and 2-min closed microwave irradiation. The optimal reaction conditions that can reach 97.7% of conversion rate were amount of catalyst used, 1.0 wt%; reaction temperature, 333 K; and methanol/oil molar ratio, 6:1.

Research article   ○   Abstract only

Concentrations and modes of occurrence of platinum group elements in the Shengli River oil shale, northern Tibet, China

Xiugen Fu, Jian Wang, Yuhong Zeng, Fuwen Tan, Jianglin He
Pages 3623-3629

⬇ Purchase PDF   Article preview ⌃

Abstract

higher than that of USA coals. PGEs in oil shale samples from the Shengli River area are characterized by high Pd (average 0.82 ng/g), Os (average 0.15 ng/g) and Pt (average 0.66 ng/g) contents compared with Ru (average 0.05 ng/g), Rh (average 0.05 ng/g) and Ir (average 0.02 ng/g). Distribution patterns of individual PGEs are not uniform in the Shengli River oil shale section. The lower marl layer is characterized by the highest Ru and Rh concentrations, whereas the upper marl layer is characterized by the highest Os and Ir concentrations. The highest Pt and Pd concentrations are found in the lower and upper parts of oil shale seams, respectively.

The individual PGEs in the oil shale samples from the Shengli River area exhibit various modes of occurrence. Ru is mainly present in P-bearing minerals and partly associated with the clay and Ca-

Research article   ○   Abstract only

Preparation of mullite from desilication-flyash

Anran Guo, Jiachen Liu, Rui Xu, Hai Xu, Caifen Wang

Pages 3630-3636

⤓ Purchase PDF   Article preview ∧

Abstract

A novel technique of flyash utilization was presented and mullite ceramics were prepared from flyash and desilication-flyash. The effect of desilication process was analyzed and the result shows that the only difference between flyash and desilication-flyash lies in the silica content, which is caused by the removal of silicate glassy phase during the desilication process. The physical and mechanical properties of flyash sample and desilication-flyash samples were measured. All results indicate that the desilication-flyash is more suitable to be used to prepare the mullite ceramics than flyash. The inner structure of flyash particle was first discovered, which can help us form a new description of the flyash particle and finally benefit the utilization of flyash. Lath-like mullite crystals appeared in high-iron samples and needle-like mullite crystals were observed in low-iron

Research article ○ Abstract only

Fuel consumption and emissions from a diesel power generator fuelled with castor oil and soybean biodiesel

Osmano Souza Valente, Márcio José da Silva, Vanya Márcia Duarte Pasa, Carlos Rodrigues Pereira Belchior, José Ricardo Sodré

Pages 3637-3642

⤓ Purchase PDF   Article preview ∧

Abstract

biodiesel in diesel oil, and fuel blends containing 5%, 20%, and 35% of castor oil biodiesel in diesel oil were tested, varying engine load from 9.6 to 35.7 kW. Specific fuel consumption (SFC) and the exhaust concentrations of carbon dioxide (CO_2), carbon monoxide (CO), and hydrocarbons (HC) were evaluated. The engine was kept with its original settings for diesel oil operation. The results showed increased fuel consumption with higher biodiesel concentration in the fuel. Soybean biodiesel blends showed lower fuel consumption than castor biodiesel blends at a given concentration. At low and moderate loads, CO emission was increased by nearly 40% and over 80% when fuel blends containing 35% of castor oil biodiesel or soybean biodiesel were used,

respectively, in comparison with diesel oil. With the load power of 9.6 kW, the use of fuel blends containing 20% of castor oil biodiesel or soybean biodiesel increased HC emissions by 16% and

Research article ○ Abstract only

CFD study of a sudden-expanding coal combustor using Euler–Euler and Euler–Lagrange models

Yu Zhang, Xiao-Lin Wei, Da-You Liu

Pages 3643-3649

⬇ Purchase PDF   Article preview ∧

Abstract

Abstract

In this study, the Euler–Euler (E–E) and Euler–Lagrange (E–L) models designed for the same chemical mechanism of heterogeneous reactions were used to predict the performance of a typical sudden-expanding coal combustor. The results showed that the current E–E model underestimated the coal burnout rate because the particle temperature fluctuation on char combustion is not adequately considered. A comparison of the E–E and E–L simulations showed the underestimation of heterogeneous chemical reaction rates by the E–E model.

Research article ○ Abstract only

A comprehensive mathematical model for biomass gasification in a bubbling fluidized bed reactor

Priyanka Kaushal, Jalal Abedi, Nader Mahinpey

Pages 3650-3661

⬇ Purchase PDF   Article preview ∧

Abstract

A mathematical model of biomass gasification in bubbling fluidized gasifier has been developed. It is a one-dimensional, two-phase (bubble and emulsion), two-zone (bottom dense bed and upper freeboard), steady state model. The model is based on global reaction kinetic, mass and energy balances and is capable of predicting temperature, solid hold ups and gas concentration along the

reactor's major axis. The overall model has sub-models to deal with biomass pyrolysis, gasification, bed hydrodynamics, material classification and property calculation. A sub-model for tar generation and cracking is included in this study. The model is capable of dealing with wide variety of biomasses and fluidizing agents, i.e. air, oxygen, steam or a mix of these gases. Results show that during devolatilization step, gases release and mixing are sensitive and critical parameters. They have a strong influence on the overall performance of a gasifier. A comparison

Research article ○ Abstract only

2009 Quality survey of retail biodiesel blends in Michigan

Rhet C. de Guzman, Haiying Tang, Sachinta Wadumesthrige, Tim Zhou, … Steven O. Salley
Pages 3662-3667

⭳ Purchase PDF   Article preview ⌃

Abstract

A fuel quality survey of biodiesel blends collected in June 2009 from 20 Michigan retail stations was performed, 8 months after the publication of ASTM D7467. Measured blend levels were not consistent in stations where pump labels indicate specific biodiesel blend levels. Fatty acid methyl ester (FAME) analyses revealed that majority of the samples are soybean oil-based (SBO) biodiesel. Full compliance with the ASTM D7467 requirements for kinematic viscosity and flash point (FP) were observed with the biodiesel blends; all but one for cetane number (CN). Barely half of the samples were able satisfy the total acid number (TAN) specification with select samples reflecting as high as 1.6 mg KOH/g. The most pressing is that only 45% were able to meet the 6 h induction period (IP) requirement; out of those that did not qualify 42% are even low blends hinting the degraded quality of the biodiesel component. Inconsistencies on the expected correlations of the tested properties were evident, suggesting that additives may be present in many samples. When

Research article ○ Abstract only

Study on the phosphate removal from aqueous solution using modified fly ash

Ke Xu, Tong Deng, Juntan Liu, Weigong Peng
Pages 3668-3674

⭳ Purchase PDF   Article preview ⌃

Abstract

that modification of fly ash could significantly enhance the phosphate immobilization ability of the fly ash. The specific surface area of the fly ash increased from 8.8 to 32.5 m^2/g after treated with sulfuric acid. The modification of the fly ash also resulted in the mobilization of acid-soluble metal ions due to partial or complete dissolution of the metals under the acidic conditions. Both adsorption and precipitation contributed to the removal of phosphate by the modified fly ash but precipitation was a major mechanism of phosphate removal. The experimental results showed that adsorption of phosphate by the modified fly ash was rapid, the removal percentage of phosphate could reach maximum in 5 min. In the range of 5–9, pH did not significantly affect the removal of phosphate and the removal percentage of phosphate increased with the increase of adsorbent dosage. The adsorption of phosphate by the modified fly ash could be described well by Langmuir

Research article ○ Abstract only

Synthesis of biodiesel from edible, non-edible and waste cooking oils via supercritical methyl acetate transesterification

Pasquale Campanelli, Mauro Banchero, Luigi Manna

Pages 3675-3682

⬇ Purchase PDF　　　Article preview ∧

Abstract

Abstract

The use of methyl acetate instead of methanol for supercritical synthesis of glycerol-free biodiesel from vegetable oils is a new process and its study is very limited in the literature. In this work, it has been tested for the first time on three edible and non-edible oils with different fatty acid composition. The process was also applied to waste oil with higher free fatty acid (FFA) content. The results demonstrate that the oil composition does not significantly influence the biodiesel yield.

The influence of temperature, pressure and molar ratio of reactants was studied. All the oils achieved complete conversion after 50 min at 345 °C, 20 MPa with methyl acetate:oil molar ratio

Research article ○ Abstract only

Determination of the reactive component of fly ashes for geopolymer production using XRF and XRD

Ross P. Williams, Arie van Riessen

Pages 3683-3692

 Purchase PDF   Article preview ∧

Abstract

determining the formulation of geopolymers to get the desired matrix chemistry uses the bulk composition of the feedstock materials. This formulation method is widely used in investigations using feedstock materials that almost completely react during processing. It is widely considered that amorphous components of fly ash are the reactive components in the geopolymerisation reaction. However, quantification of the amorphous components is challenging and generally avoided with the concomitant problem that the formulation is far from optimum. For the work presented here, the composition of the amorphous part is determined accurately and this information utilised to synthesise geopolymers. The bulk composition is first determined using X-ray fluorescence spectroscopy (XRF) and then the amorphous composition determined using XRF and quantitative X-ray diffraction (QXRD). Formulating the mixture based on amorphous

Research article ○ Abstract only

Numerical investigation of Solid Recovered Fuels' co-firing with brown coal in large scale boilers – Evaluation of different co-combustion modes

Michalis Agraniotis, Nikos Nikolopoulos, Aris Nikolopoulos, Panagiotis Grammelis, Emmanuel Kakaras

Pages 3693-3709

 Purchase PDF   Article preview ∧

Abstract

Abstract

In the current work the co-combustion of Solid Recovered Fuels' (SRFs') with brown coal in large scale pulverised coal boilers under different operational conditions is numerically investigated. In order to overcome the difficulty of the complex, inhomogeneous nature of waste recovered fuels, SRF is modelled as a mixture of two different fractions, the biogenic and the plastic one. For each fraction different combustion mechanisms are presented, whilst for the first time the proposed

combustion mechanism of the plastic fraction is incorporated in a commercial CFD code and validated against available experimental data. A 600 MW_e brown coal boiler is simulated as a reference and its operational characteristics are compared with parameterised scenarios of SRF co-

Research article ○ Abstract only

Correlations for dependence of NO_x emissions on heat loss in premixed CH_4/air combustion

Cheol-Hong Hwang, Chung-Hwa Park, Seul-Hyun Park

Pages 3710-3717

⤓ Purchase PDF   Article preview ∧

Abstract

using a perfectly stirred reactor (PSR) code. The numerical results showed that the calculated NO_x concentration initially increased, reached a maximum value and then decreased with increasing residence time when the heat loss was present. The similar variation was observed in changes in the thermal NO concentration that was evaluated by only considering the reactions associated with the thermal (Zeldovich) NO mechanism. With the heat loss increased, the calculated NO_x concentration was substantially reduced for all equivalence ratios investigated. In addition, the reductions in the NO_x concentration with respect to residence time became faster with increasing the equivalence ratio particularly for fuel rich conditions. The observed variations in the calculated NO_x concentration over the residence time (NO_x/τ) were found to fit well to the following correlation: $\ln(NO_x/\tau) = a(HLI) + b$. In the correlation, HLI is the dimensionless heat loss

Research article ○ Abstract only

Sunflower biodiesel production and application in family farms in Brazil

Anderson Favero Porte, Rosana de Cassia de Souza Schneider, Jonas Alvaro Kaercher, Rodrigo Augusto Klamt, ... Wolmar Alípio Severo Filho

Pages 3718-3724

⤓ Purchase PDF   Article preview ∧

Abstract

Abstract

There are limited options available for compact small-scale biodiesel production equipment that produces biodiesel of similar quality as that obtained from an industrial-scale production system. The aim of the present study was to evaluate equipment optimization for producing 40–200 L/day of biodiesel. The equipment was used to produce biodiesel for personal consumption. The produced biodiesel was tested in three microtractors, the principal agricultural machines used in family farms in the Vale do Rio Pardo region of Southern Brazil. Our results demonstrated that the equipment produced biodiesel of sufficient quality according to the limits established by the Brazilian Petroleum National Agency (ANP). In conclusion, this biodiesel can be used in microtractors with little wear on engine parts.

Research article ○ Abstract only

Forage turnip, sunflower, and soybean biodiesel obtained by ethanol synthesis: Production protocols and thermal behavior

C.M. Soares, L.C.V. Itavo, A.M. Dias, E.J. Arruda, ... L.C.S. de Oliveira

Pages 3725-3729

⬇ Purchase PDF　　　Article preview ⌃

Abstract

Abstract

In this work it is reported a detailed investigation of the effect of different production protocols based on alkaline ethanolysis on conversion yield of forage turnip, soybean, sunflower, and castor oil into the respective biodiesel. Parameters such as catalyst contents, reaction times and temperatures were evaluated. Additionally, it was also investigated the relationship between the conversion yield and the chemical composition of the fatty acids in the feedstock. Conversion yields ranging between 70% and 100% point out the viability of the production of biodiesel using ethanol. Based on thermal analysis, sequential steps of weight loss were observed indicating that biodiesel undergoes oxidative thermal decomposition with the elimination of different portions of the molecules in each step. Besides, the energies released by the samples during thermal

Research article ○ Abstract only

Tracking aromaticity changes in heavy hydrocarbon processing by monitoring changes in electrical resistivity

Clovis Bombardelli, Lívia Mari Assis, Hypolito José Kalinowski

⬇ Purchase PDF   Article preview ︿

Abstract

Abstract

In this work, the changes in electrical resistivities of a vacuum residuum are analyzed to determine pyrolysis reaction rates at different temperatures during high temperature processing. Fractions of the residual oil from vacuum distillation were treated at a constant and uniform temperature, and electrical resistance was related to aromaticity. The results show that resistivity behaves like a first order decay-like thermal cracking reaction. This method could replace chemical methods used to determine the temperature necessary for thermal cracking reactions and the kinetic parameters of heavy petroleum fractions.

Research article ○ Abstract only

Atomization and combustion of canola methyl ester biofuel spray

Jaime A. Erazo, Ramkumar Parthasarathy, Subramanyam Gollahalli

⬇ Purchase PDF   Article preview ︿

Abstract

Abstract

The spray atomization and combustion characteristics of canola methyl ester (CME) biofuel are compared to those of petroleum based No. 2 diesel fuel in this paper. The spray flame was contained in an optically accessible combustor which was operated at atmospheric pressure with a co-flow of heated air. Fuel was delivered through a swirl-type air-blast atomizer with an injector orifice diameter of 300 μm. A two-component phase Doppler particle analyzer was used to measure the spray droplet size, axial velocity, and radial velocity distributions. Radial and axial distributions of NO, CO, CO_2 and O_2 concentrations were also obtained. Axial and radial distributions of flame

temperature were recorded with a Pt–Pt/13%Rh (type R) thermocouple. The volumetric flow rates
~~of fuel atomization air and co-flow air were kept constant for both fuels. The droplet Sauter mean~~

Research article ○ Abstract only

Thermal analysis of a diesel engine operating with diesel–biodiesel blends

Marcelo J. Colaço, Cláudio V. Teixeira, Luciana M. Dutra

Pages 3742-3752

⬇ Purchase PDF　　　Article preview ∧

Abstract

Abstract

In this paper we study the transient heat conduction in a piston of a diesel engine, subjected to a periodic boundary condition on the surface in contact with the combustion gases. The heat transfer coefficient at the top surface was modeled taking into account the temperature and pressure inside the combustion chamber. Such instantaneous pressure was measured using a special probe for an engine operating with several blends of diesel and biodiesel, and the temperature was obtained through a First Law analysis. The physical properties, including the cetane number were evaluated experimentally for all diesel/biodiesel blends used in this work. An elliptic scheme of numerical grid generation was used, so that the irregular shaped piston in the ~~physical domain was transformed into a cylinder in a computational domain. The timewise~~

Research article ○ Abstract only

An investigation of the catalytic abatement of emissions from the combustion of diesel/bioethanol blends

Grisel Corro, Edgar Ayala, Nallely Tellez, Mario M. Bustillo Diaz

Pages 3753-3757

⬇ Purchase PDF　　　Article preview ∧

Abstract

Abstract

In this study, we investigated the activity of pre-sulfated $1\%Pt–2\%Sn/\gamma–Al_2O_3$ on the catalytic abatement of the combustion emissions of three fuels: pure diesel E(0), pure bioethanol E(100) and

bioethanol blended diesel containing 10% bioethanol E(10). The emissions generated, by each blend combustion, were conducted continuously to the catalyst sample. The catalytic activity was determined by following the evolution of the outflow emissions concentrations by FTIR gas spectroscopy as a function of the catalyst temperature. Results showed that the addition of bioethanol to diesel may be necessary to enhance the catalytic oxidation of diesel unburned hydrocarbons and particulate matter on pre-sulfated $1\%Pt–2\%Sn/\gamma–Al_2O_3$.

Research article ○ Abstract only

Simulation and analysis of group-hole nozzle sprays using a gas jet superposition model

Jian Gao, Sung Wook Park, Yue Wang, Rolf D. Reitz, … Keiya Nishida
Pages 3758-3772

⬇ Purchase PDF   Article preview ⌃

Abstract

Abstract

A gas jet superposition model has been recently developed for computing group-hole nozzle sprays in computational fluid dynamics (CFD) simulations. The objectives of this study are: (1) to perform a systematic validation of the comprehensive spray model for group-hole nozzles using a broad range of experimental data; (2) to analyze the dynamics and physical insight of group-hole nozzle sprays based on the simulation results; and (3) to further clarify the impact of included-angle on spray/mixture properties of group-hole nozzle sprays. An updated version of the KIVA-3V Release 2 code, which employs the Lagrangian-Drop Eulerian-Fluid (LDEF) methodology for numerical calculation of two-phase flows, was used in the simulations. Diverging group-hole nozzles with various included-angles were considered. The test conditions included non-evaporating and

Research article ○ Abstract only

Biomass direct chemical looping process: Process simulation

Fanxing Li, Liang Zeng, Liang-Shih Fan
Pages 3773-3784

⬇ Purchase PDF   Article preview ⌃

Abstract

Abstract

Biomass is a clean and renewable energy source. The efficiency for biomass conversion using conventional fuel conversion techniques, however, is constrained by the relatively low energy density and high moisture content of biomass. This study presents the biomass direct chemical looping (BDCL) process, an alternative process, which has the potential to thermochemically convert biomass to hydrogen and/or electricity with high efficiency. Process simulation and analysis are conducted to illustrate the individual reactor performance and the overall mass and energy management scheme of the BDCL process. A multistage model is developed based on ASPEN Plus® to account for the performance of the moving bed reactors considering the reaction equilibriums. The optimum operating conditions for the reactors are also determined. Process

Research article ○ Abstract only

Evaluation of guindilla oil (*Guindilia trinervis* Gillies ex Hook. et Arn.) for biodiesel production

Ricardo San Martín, Teófilo de la Cerda, Adolfo Uribe, Paola Basilio, … Marlene Gebauer

Pages 3785-3790

⬇ Purchase PDF   Article preview ∧

Abstract

Abstract

Guindilla plants (*Guindilia trinervis* Gillies ex Hook. et Arn.) are small shrubs that grow wildly in the mountains of Central Chile in soils and climates not suitable for agriculture. Whole guindilla seeds contain 28–29% w/w oil. Cotyledons represent 45% w/w of the seed and contain 63–64% w/w oil. Main unsaturated fatty acids are oleic (63% w/w), linoleic (8% w/w) and gadoleinic (9.5% w/w), while main saturated fatty acids are palmitic (9.1% w/w) and stearic (3.1% w/w). The content of free fatty acids was 0.06%. Transesterification reactions yielded a biodiesel with ester content >99%; cetane number 59; oxidative stability at 110 °C, 18.9 h; kinematic viscosity at 40 °C, 4.867 mm^2/s; cold filter plugging point, CFPP + 4 °C; sulfur content 1.0 mg/kg; sulfated ash < 0.01% p/p; acid value 0.024 mg KOH/g and phosphorous content (<0.5 mg/kg). All values were within European and US

Research article ○ Abstract only

Biodiesel production by ethanolysis of mixed castor and soybean oils

Daniela da Costa Barbosa, Tatiana M. Serra, Simoni M. Plentz Meneghetti, Mario R. Meneghetti
Pages 3791-3794

⤓ Purchase PDF   Article preview ⌃

Abstract

Abstract

Biodiesel was produced by ethanolysis of pure castor and soybean oils, and mixtures thereof, using potassium hydroxide as catalyst. The yields and selectivities of these reactions were evaluated. The results revealed that there was no appreciable substrate preference when the vegetable oils were transesterified in admixture. However, higher reaction yields and increased efficiencies of the purification process were directly correlated with the proportion of soybean oil present in the reaction mixture.

Research article ○ Abstract only

Modelling of an updraft fixed-bed gasifier operated with softwood pellets

C. Mandl, I. Obernberger, F. Biedermann
Pages 3795-3806

⤓ Purchase PDF   Article preview ⌃

Abstract

Abstract

This paper presents a one-dimensional steady state mathematical model for the simulation of a small scale fixed-bed gasifier. The model is based on a set of differential equations describing the entire gasification process of softwood pellets and is solved by a two step iterative method. The main features of the model are: homogeneous and heterogeneous combustion and gasification reactions, one-step global pyrolysis kinetics and drying, heat and mass transfer in the solid and gas phases as well as between phases, heat loss, particle movement and shrinkage within the bed. The pyrolysis model has been improved by partially cracking primary tar into lighter gases according to experimental data. The model is used to simulate a laboratory scale fixed-bed updraft gasifier.

Research article ○ Abstract only

Limitations of the use of cetane index for alternative compression ignition engine fuels

Noel Bezaire, Kapila Wadumesthrige, K.Y. Simon Ng, Steven O. Salley

⬇ Purchase PDF　　　Article preview ⌃

Abstract

Abstract

The cetane number of a fuel is an important factor in determining the quality of ignition in compression ignition (CI) engines. The significance of accurate measurement of cetane number has become even greater since the use of alternative fuels and modern CI engines. In this work, the comparison of different methods of cetane value measurement for fuels with different chemical composition such as ultra low sulfur diesel (ULSD), synthetic jet fuel (S-8) and military grade jet fuel (JP-8), trace amounts of additives and biodiesel blends under different conditions is reported. The cetane index was calculated by ASTM D4737 and ASTM D976 and the derived cetane number (DCN) was measured using an Ignition Quality Tester (IQT) as a basis of comparison with the cetane index. The best agreement among three methods was observed for ULSD, while S-8 showed

Research article ○ Abstract only

Investigation of the combustion of neat cottonseed oil or its neat bio-diesel in a HSDI diesel engine by experimental heat release and statistical analyses

C.D. Rakopoulos, D.C. Rakopoulos, E.G. Giakoumis, A.M. Dimaratos

⬇ Purchase PDF　　　Article preview ⌃

Abstract

Abstract

An experimental study is conducted to evaluate the effects of using neat cottonseed oil or its neat ME (methyl ester) bio-diesel, on the combustion behavior of a standard, high speed, direct injection (HSDI), 'Hydra' diesel engine located at the authors' laboratory. Combustion chamber and

fuel injection pressure diagrams are obtained at medium and high load using a developed, high-speed, data acquisition and processing system. A heat release analysis of the experimentally obtained cylinder pressure diagrams is developed and used. Plots of histories in the combustion chamber of the heat release rate and other related parameters reveal some interesting features, which shed light into the combustion mechanism when using these bio-fuels. These results,

Research article ○ Abstract only

Performance and emission characteristics of an CI engine fueled with diesel–biodiesel–bioethanol blends

István Barabás, Adrian Todoruţ, Doru Bǎldean
Pages 3827-3832

⤓ Purchase PDF   Article preview ⌃

Abstract

Abstract

The paper presents the experimental results obtained concerning performances and pollution of a diesel engine fueled with diesel–biodiesel–ethanol blends compared with diesel fuel in laboratory tests. The main properties of the researched fuels are presented within this paper, in comparison with classical diesel fuel (chemical composition, density, kinematic viscosity, cold filter plugging point, flash point). Engines' performances were evaluated by determining the brake specific fuel consumption and brake thermal efficiency. For pollution evaluation the emissions of CO, CO_2, NO_x, HC and smoke have been measured. An increasing of brake specific fuel consumption has been observed, especially at lower engines' loads, with maximum 32.4%, reducing engine brake thermal efficiency with maximum 21.7%. CO emissions decrease, especially at high loads with

Research article ○ Abstract only

Optimization of supercritical dimethyl carbonate (SCDMC) technology for the production of biodiesel and value-added glycerol carbonate

Kok Tat Tan, Keat Teong Lee, Abdul Rahman Mohamed
Pages 3833-3839

⤓ Purchase PDF   Article preview ⌃

Abstract

Abstract

In the present study, biodiesel has been successfully produced from triglycerides and dimethyl carbonate, instead of the conventional alcohol. In this non-catalytic supercritical dimethyl carbonate (SCDMC) technology, valuable compound of glycerol carbonate is obtained as side product, rather than the undesirable glycerol. Glycerol carbonate has higher commercial value compared to glycerol and its application in industries is enormous. In this optimization study, the effects of important parameters including reaction temperature, molar ratio of dimethyl carbonate to oil and reaction time were investigated and optimized by employing response surface methodology (RSM) analysis. It was found that the mathematical model developed was statistically significant and adequate to predict the optimum yield. The optimum conditions for SCDMC

Research article   ○ Abstract only

Emission characteristics of diesel, gas to liquid, and biodiesel-blended fuels in a diesel engine for passenger cars

Gunfeel Moon, Yonggyu Lee, Kyonam Choi, Dongsoo Jeong

Pages 3840-3846

⬇ Purchase PDF   Article preview ⌃

Abstract

Abstract

The need for diversification of energy sources and reducing various emissions including CO_2 emission in diesel engine can be met with alternative diesel fuels such as gas to liquid (GTL) and GTL–biodiesel blends. But there should be a clear understanding of the combustion and engine-out emission characteristics for alternative fuels. In this respect, an experimental study was conducted on a 2.0 L 4 cylinders turbocharged diesel engine fuelled with those alternative diesel fuels to investigate the engine-out emission characteristics under various steady-state engine operating conditions. The results revealed that noticeable decreases in THC (22–56%) and CO (16–52%) emissions for GTL–biodiesel blends were observed, whereas NOx emissions for GTL–biodiesel blends increased by a maximum of 12% compared to diesel. With regard to particle size

Research article ○ Abstract only

Effect of MEA fabrication techniques on the cell performance of Pt–Pd/C electrocatalyst for oxygen reduction in PEM fuel cell

Sarawalee Thanasilp, Mali Hunsom

Pages 3847-3852

⬇ Purchase PDF   Article preview ⌃

Abstract

Abstract

The effect of three different membrane electrode assembly (MEA) fabrication techniques, catalyst-coated substrate by direct spray (CCS) and catalyst-coated membrane by direct spray (CCM-DS) or decal transfer (CCM-DT), on the performance of oxygen reduction in a proton exchange membrane (PEM) fuel cell was carried out under identical conditions of Pt–Pd/C electrocatalyst loading. The results indicated that the fabrication technique had only a very slight effect on the ohmic resistance of the PEM fuel cell but it significantly affected the charge transfer resistance and open circuit voltage (OCV). The cells prepared by the CCM method, and particularly by decal transfer, exhibited a significantly higher OCV but a lower ohmic and charge transfer resistance compared with the other investigated fabrication techniques. By using cyclic voltammetry with H_2 adsorption, it was

Research article ○ Abstract only

Fly ash-supported cerium triflate as an active recyclable solid acid catalyst for Friedel–Crafts acylation reaction

Chitralekha Khatri, Deepti Jain, Ashu Rani

Pages 3853-3859

⬇ Purchase PDF   Article preview ⌃

Abstract

Abstract

An efficient solid Lewis acid, has been synthesized by loading cerium triflate (7 wt%) on the acid activated fly ash with high silica content (81%). The physico-chemical properties of synthesized fly ash-supported cerium triflate catalyst (CFT) were monitored by XRD, FT-IR spectroscopy, FT-IR spectroscopy of the ammonia adsorbed catalyst, SEM-EDAX, TEM, Flame Atomic Absorption

Spectrophotometer and TG-DTA study. The increased concentration of silica surface hydroxyl groups on activated fly ash have a major influence on the loading of cerium triflate. The catalytic activity of the catalyst CFT was tested in the acylation of veratrole using acetic anhydride as the acylating agent. The proposed model structure of CFT shows that the triflate species withdraws the

Research article ○ Abstract only

Stabilization of water-in-octane nano-emulsion. II Enhanced by amphiphilic graft copolymers based on poly (higher α-olefin)-*graft*-poly(ethylene glycol)

Zhisheng Fu, Min Liu, Junting Xu, Qi Wang, Zhiqiang Fan

Pages 3860-3865

⤓ Purchase PDF   Article preview ⌃

Abstract

Abstract

Previously water-in-octane nano-emulsions were prepared by mixed surfactant systems. In this paper, a series of amphiphilic graft copolymers, namely poly (higher α-olefin-*co-para*-methylstyrene)-*graft*-poly(ethylene glycol) and poly (higher α-olefin-*co*-acrylic acid)-*graft*-poly(ethylene glycol), were used as additives to enhance the stability of these nano-emulsions. Although the amphiphilic graft copolymers did not impact the average diameter of the water droplets in these emulsions to a major extent, the stability of these emulsions were enhanced significantly by the interaction between surfactants and amphiphilic graft copolymers. Amphiphilic graft copolymers' stabilizing capability depends on their chain structure and composition. In a proper range of poly(ethylene glycol) content, e.g. 6.0–34.0 wt.%, the higher the

Research article ○ Abstract only

Accelerating transesterification reaction with biodiesel as co-solvent: A case study for solid acid sulfated tin oxide catalyst

Man Kee Lam, Keat Teong Lee

Pages 3866-3870

⤓ Purchase PDF   Article preview ⌃

Abstract

Abstract

Solid acid catalysts are normally used to catalyze the transesterification of oil with high free fatty acid (FFA) to biodiesel. However, the immiscible phases of methanol-oil-catalyst in the initial reaction mixture usually lead to slow reaction rate and long reaction time. One possible way to overcome this limitation is by using co-solvent that has high solubility in oil and methanol. Therefore, in the present study, the use of biodiesel as co-solvent for transesterification reaction catalyzed by $SO_4^{2-}/SnO_2–SiO_2$ (solid acid catalyst) was investigated. It was found that with the use of biodiesel as co-solvent, a high FAME yield of 88.2% (almost 30% higher than without using co-solvent) can be obtained in a shorter reaction time (1.5 h) using the following reaction conditions; reaction temperature of 150 °C, methanol to oil ratio of 15 and catalyst loading of 6 wt.% (weight of

Research article ○ Abstract only

Low boiling point organic amine-catalyzed transesterification of cottonseed oil to biodiesel with trace amount of KOH as co-catalyst

Jianfeng Yao, Lei Ji, Peiyong Sun, Lixiong Zhang, Nanping Xu
Pages 3871-3875

⤓ Purchase PDF   Article preview ∧

Abstract

Abstract

The effect of addition of trace amount of KOH as co-catalyst on low boiling point organic amine-catalyzed transesterification for biodiesel production was investigated. Three different organic amines, tri-ethylamine, di-ethylamine and tert-butylamine, were used as catalysts, and the maximum amount of KOH that could be added to these organic amine-catalyzed systems was 367.1 mg/kg oil. Under such circumstance, KOH could be left in the resultant biodiesel and no washing was needed to remove it as the concentration of K^+ in the biodiesel met EN 14214 standards. Addition of trace amount of co-catalyst KOH with an amount of 367.1 mg/kg oil resulted in the organic amine-catalyzed transesterification under milder reaction conditions than those without addition of KOH to achieve >90% yield of methyl ester. Furthermore, side reactions

Research article ○ Abstract only

The impact of soy-based biodiesel on PAH, nitro-PAH and oxy-PAH emissions from a passenger car operated over regulated and nonregulated driving cycles

George Karavalakis, George Deves, Georgios Fontaras, Stamoulis Stournas, … Evangelos Bakeas

Pages 3876-3883

⬇ Purchase PDF　　　Article preview ⌄

Abstract

Abstract

This study explores the impact of neat soy-based methyl ester and its 50% v/v blend with low sulphur automotive diesel on PAH, nitro-PAH and oxy-PAH emissions of a Euro 2 compliant diesel passenger car tested on a chassis dynamometer. Emission measurements were evaluated for the certification NEDC, a hot-start UDC (urban part of NEDC) and the non-legislated Artemis driving cycles which simulate urban, rural and highway driving conditions in Europe. Overall, 16 PAHs, 4 nitro-PAHs and 6 oxy-PAHs were determined in the exhaust. The results obtained, showed that PAH emissions decreased with the addition of biodiesel during all driving modes. However, their nitrated and oxygenated products were found to increase with biodiesel compared to diesel fuel. The use of pure biodiesel led in some increases in PAH emissions when compared to

---

Research article ○ Abstract only

Morphological characterization of super fine pulverized coal particle. Part 2. AFM investigation of single coal particle

Jiaxun Liu, Xiumin Jiang, Xiangyong Huang, Shaohua Wu

Pages 3884-3891

⬇ Purchase PDF　　　Article preview ⌄

Abstract

Abstract

Super fine pulverized coal combustion is a new pulverized coal combustion technology which has better stability, higher combustion efficiency and lower NO_x and SO_2 emission than that using conventional particle sizes. In this paper we applied fractal analysis based on power spectral density (PSD) and slit island method (SIM), three-dimensional (3D) surface roughness measurement and surface-topography observations from AFM to form a proper investigative tool

which may give a relatively full picture of surface morphology of super fine pulverized coal particles for the first time. The final results indicate that both fractal dimensions calculated by SIM and PSD and roughness of coal particle size increase with the increase of the coal particle size.

Research article ○ Abstract only

Radiological characteristics of pulverized fly ashes produced in Turkish coal-burning thermal power plants

Ş. Turhan, A. Parmaksız, A. Köse, A. Yüksel, … B. Yücel
Pages 3892-3900

⤓ Purchase PDF　　　Article preview ⌃

Abstract

Abstract

The objective of this study is to determine radiological characteristics of pulverized fly ash (PFA) collected from the 15 coal-burning thermal power plants (TPPs) in operation by means of gamma spectrometric technique and to assess the radiological impacts from the utilization of PFA samples examined as filling and cover material in earthwork applications. Also, the annual effective doses received by workers handling PFA and members of the public living in a house near the PFA pile/landfill were estimated using methods specified in the Radiation Protection 122. The activity concentrations of ^{226}Ra, ^{232}Th and ^{40}K measured in PFA samples were tabulated for each TPP. The activity results show that Turkish PFA may have relatively high natural radioactivity content, depending on its origin reaching in the case of Kangal PFA 2720 Bq kg^{-1} of ^{226}Ra. The values of

Research article ○ Abstract only

Two-stage equilibrium model applicable to the wide range of operating conditions in entrained-flow coal gasifiers

Thanh D.B. Nguyen, Young-Il Lim, Byung-Ho Song, Si-Moon Kim, … Dal-Hong Ahn
Pages 3901-3910

⤓ Purchase PDF　　　Article preview ⌃

Abstract

Abstract

A two-stage equilibrium model applicable to the wide range of operating conditions is developed to predict carbon conversion and composition of the product gas in an entrained-flow coal gasifier. The model is composed of two separate stages including char-gasification and gas-phase reaction. Carbon conversion is estimated in the first stage with solid–gas reactions, and then the product gas composition is calculated from gas-phase reactions in the second stage. Water consumption involved in the equilibrium reaction of the first stage is expressed as an exponential function of temperature. The model is validated with experimental data taken from literatures. It is confirmed that carbon conversion and product gas composition are influenced significantly by the oxygen to coal ratio. The optimum range of steam to coal ratio and the total yield of CO and H_2 depend on

Research article   ○   Abstract only

An investigation of the grindability of two torrefied energy crops

T.G. Bridgeman, J.M. Jones, A. Williams, D.J. Waldron

Pages 3911-3918

⤓ Purchase PDF   Article preview ∧

Abstract

Abstract

The process of torrefaction alters the physical properties of biomass, reducing its fibrous tenacious nature. This could allow increased rates of co-milling and therefore co-firing in coal fired power stations, which in turn would enable a reduction in the amount of coal used and an increase in the use of sustainable fuels, without the need for additional plant. This paper presents an experimental investigation of the pulverisation behaviour of two torrefied energy crops, namely: willow and Miscanthus. A multifactorial method approach was adopted to investigate the three process parameters of temperature, residence time and particle size, producing fuels treated using four different torrefaction conditions. The untreated and torrefied fuels were subjected to standard fuel analysis techniques including ultimate analysis, proximate analysis and calorific value

Research article   ○   Abstract only

Effect of injection and ignition timings on performance and emissions from a spark-ignition engine fueled with methanol

Jun Li, Chang-Ming Gong, Yan Su, Hui-Li Dou, Xun-Jun Liu
Pages 3919-3925

⬇ Purchase PDF   Article preview ⌃

Abstract

Abstract

Optimal injection and ignition timings and the effects of injection and ignition timings on performance and emissions from a high-compression direct-injection stratified charge spark-ignition methanol engine have been investigated experimentally. The results have shown that direct-injection spark-ignition methanol engine, in which a non-uniform mixture with a stratified distribution can be formed, has optimal injection and ignition timings to obtain a good combustion and low exhaust emissions in the overall mode range. Both methanol injection timing and ignition timing have a significant effect on methanol engine performance, combustion, and exhaust emissions. At an engine speed of 1600 rpm, full load, and optimal injection and ignition timings, methanol engine can obtain shorter ignition delay, lesser cycle-by-cycle variation, the

Research article   ○   Abstract only

A direct numerical simulation study of coherent oscillation effects of swirling flows

Nan Gui, JianRen Fan, Kefa Cen, Song Chen
Pages 3926-3933

⬇ Purchase PDF   Article preview ⌃

Abstract

Abstract

In this study, we carried out a direct numerical simulation of swirling jets to investigate the temporal characteristics of coherent structures related to the vortex breakdown. The type of coherent motion of oscillation, as a temporal characteristic of vortex breakdown, is observed through the analysis of correlation functions. It indicates that the vortex breakdown is accompanied with the resonance of fluctuations of flow velocity, pressure, vortices and etc. Moreover, it is found that the coherent oscillation occurs only for the swirling flows with a high

level of swirl (larger than the critical value) when the bubble vortex breakdown takes place, and only

Research article ○ Abstract only

The effect of hydrothermal dewatering of Pontianak tropical peat on organics in wastewater and gaseous products

Anggoro Tri Mursito, Tsuyoshi Hirajima, Keiko Sasaki, Satoshi Kumagai
Pages 3934-3942

⤓ Purchase PDF   Article preview ⌃

Abstract

Abstract

This paper describes a study of the effects of hydrothermal dewatering of raw tropical peat from Pontianak, West Kalimantan-Indonesia, on the amounts of organic compounds released into wastewater and gaseous products. Hydrothermal upgrading and dewatering of the peat was carried out in a batch-type autoclave reactor at temperatures between 150 and 380 °C at a maximum pressure of 25.1 MPa for 30 min. It was found that the extent of decomposition of organics during hydrothermal dewatering depended on temperature increase.

Wastewater from hydrothermal dewatering was found to contain organic carbon (TOC) ranging from 800 ppm at low temperatures, to 7504 ppm at high temperatures. A number of sugars and

Research article ○ Abstract only

Study of kinetics of co-pyrolysis of coal and waste LDPE blends under argon atmosphere

Sumedha Sharma, Aloke K. Ghoshal
Pages 3943-3951

⤓ Purchase PDF   Article preview ⌃

Abstract

Abstract

Co-pyrolysis of coal with waste plastic is increasingly being looked upon as a potential technique to counter the present day challenges in energy and waste management by harnessing the multiple

benefits associated with the same. In the present work, the kinetics of co-pyrolysis of waste LDPE carried out with coal of *Ledo* origin from the coalfields of Assam (India) has been studied. A thermo-gravimetric (TG) study of the co-pyrolysis has been carried out taking waste LDPE-coal mixtures in ratios of 3:1, 1:1, and 1:3 by weight and at five varying heating rates from 5 to 25 K min^{-1} with a 5 K increment. Experiments were also carried out for the individual components at all the five heating rates. This TG analysis data was used to evaluate the kinetics parameters such

Research article ○ Abstract only

Effect of ethanol addition in gasoline and gasoline–surrogate on soot formation in turbulent spray flames

R. Lemaire, E. Therssen, P. Desgroux

Pages 3952-3959

⬇ Purchase PDF   Article preview ∧

Abstract

Abstract

The effect of ethanol on soot formation has been studied in turbulent spray flames of gasoline/ethanol and gasoline–surrogate/ethanol mixtures containing 10%, 20% and 30% of alcohol in volume. A hybrid burner specially designed to stabilize different liquid fuels flames with identical hydrodynamic conditions has been used. Spatially resolved measurements of soot volume fraction and of soot precursors concentration have been carried out by coupling Laser-Induced Incandescence (LII) at 1064 nm and Laser-Induced Fluorescence (LIF) at 532 nm. Significant reductions of the concentrations of soot and soot precursors have been observed when adding ethanol to gasoline. A similar behaviour has been obtained with a gasoline–surrogate which has been found to reproduce well the sooting propensity of the unleaded gasoline used in this work

Research article ○ Abstract only

Synthesis and component confirmation of biodiesel from palm oil and dimethyl carbonate catalyzed by immobilized-lipase in solvent-free system

Liping Zhang, Shuzhen Sun, Zhong Xin, Boyang Sheng, Qun Liu

Pages 3960-3965

⬇ Purchase PDF   Article preview ∧

Abstract

Abstract

The transesterification of palm oil and dimethyl carbonate (DMC) for preparing biodiesel has been carried out at the catalysis of immobilized-lipase in solvent-free system. The components were all confirmed by GC and GC–MS analysis. The fatty acid methyl esters (FAMEs) were analyzed with internal standard method. The fatty acids glycerol carbonate esters (FAGCs) were characterized as the intermediates. And, glycerol dicarbonate (GDC) was confirmed as the byproduct by comparing with the model compound. Moreover, the effects of the reaction conditions (type of lipases, molar ratio of DMC and palm oil, amount of catalyst, reaction temperature and time) on the yield of FAMEs were investigated. The yield of FAMEs could reach 90.5% at 55 °C for 24 h with the molar ratio of DMC to oil 10:1 and the catalyst amount of 20% Novozym 435 (based on the oil weight)

Research article ○ Abstract only

Surface modification of high calcium fly ash for its application in oil spill clean up

O.K. Karakasi, A. Moutsatsou

⬇ Purchase PDF   Article preview ⌃

Abstract

Abstract

The present study aims at utilising an inorganic industrial by-product, high calcium fly ash (HCFA), in an environmental field: oil spill clean up. Properties, such as fine particle size, floating ability, hydrophobic character and porosity, make this material attractive for such a use. In order to investigate the oil sorption behaviour of HCFA an oil spill has been simulated, by using artificial ocean water and three types of oil (heating oil (HO), light cycle oil (LCO) and Iranian light crude oil (ILCO)). Two HCFA samples, a Ca-rich one (AD) and a Si-rich one (M), have been examined, so as to investigate the role of HCFA composition in its behaviour. The addition of HCFA to an oil spill results in the formation of a semi-solid oil–HCFA phase, allowing the quite total removal of oil from the water surface. HCFA's oil sorption capacity in dry environment after 24 h is 0.7–0.9 g oil/g

Research article ○ Abstract only

Hydrodynemics of a cocurrent upflow liquid–liquid reciprocating plate reactor for homogeneously base-catalyzed methanolysis of vegetable oils

Ivica S. Stamenković, Ivana B. Banković-Ilić, Predrag B. Jovanić, Vlada B. Veljković, Dejan U. Skala

Pages 3971-3984

Purchase PDF   Article preview ︿

Abstract

Abstract

Hydrodynamics of a continuous cocurrent two-phase upflow reciprocating plate reactor (RPR) for homogeneously base-catalyzed methanolysis of sunflower oil was studied. Here, methanol constituted the dispersed phase and sunflower oil was the continuous phase. The measurements were performed in both the non-reactive (methanol–sunflower oil) and reactive (sunflower oil–methanol–KOH) systems. The main goal was to define the effects of the vibration intensity and the important reaction operating conditions on the pressure fluctuation at the reactor bottom, the power consumption, the dispersed phase holdup, the Sauter-mean drop diameter and the specific interfacial area. The power consumption under batch, single- and two-phase flow was proved to depend on the vibration intensity. The Sauter-mean drop diameter was found to depend on the

Research article ○ Abstract only

Effect of temperature on the performance of microbial fuel cells

A. Larrosa-Guerrero, K. Scott, I.M. Head, F. Mateo, … C. Godinez

Pages 3985-3994

Purchase PDF   Article preview ︿

Abstract

Abstract

Single and double chamber microbial fuel cells (MFCs) were tested in batch mode at different temperatures ranging from 4 to 35 °C; results were analysed in terms of efficiency in soluble organic matter removal and capability of energy generation. Brewery wastewater diluted in domestic wastewater (initial soluble chemical oxygen demand of 1200 and 492 mg L^{-1} of volatile suspended solids) was the source of carbon and inoculum for the experiments. Control reactors (sealed container with support for biofilm formation) as well as baseline reactors (sealed container

with no support) were run in parallel to the MFCs at each temperature to assess the differences between water treatment including electrochemical processes and conventional anaerobic digestion (in the presence of a biofilm, or by planktonic cells). MFCs showed improvements

---

Research article ○ Abstract only

Monodisperse monocomponent fuel droplet heating and evaporation

T. Kristyadi, V. Deprédurand, G. Castanet, F. Lemoine, ... M.R. Heikal

⬇ Purchase PDF   Article preview ⌃

Abstract

Abstract

The results of numerical and experimental studies of heating and evaporation of monodisperse acetone, ethanol, 3-pentanone, n-heptane, n-decane and n-dodecane droplets in an ambient air of fixed temperature and atmospheric pressure are reported. The numerical model took into account the finite thermal conductivity of droplets and recirculation inside them based on the effective thermal conductivity model and the analytical solution to the heat conduction equation inside droplets. The effects of interaction between droplets are taken into account based on the experimentally determined corrections to Nusselt and Sherwood numbers. It is pointed out that the interactions between droplets lead to noticeable reduction of their heating in the case of ethanol, 3-pentanone, n-heptane, n-decane and n-dodecane droplets, and reduction of their cooling

---

Research article ○ Abstract only

Influence of porosity and surface groups on the catalytic activity of carbon materials for the microwave-assisted CO_2 reforming of CH_4

B. Fidalgo, A. Arenillas, J.A. Menéndez

⬇ Purchase PDF   Article preview ⌃

Abstract

Abstract

In this work, various carbon materials were studied as catalysts/microwave receptors for the CO_2 reforming of the CH_4 reaction. Carbon materials with a different textural development (metallurgical coke, activated carbons, re-activated carbon) were selected as catalysts in order to determine the role of porosity and pore size in dry reforming. Microporosity was found to be necessary for a good performance of the carbon catalysts. An activated carbon and an oxidized activated carbon were compared in order to evaluate the influence of oxygen surface groups on the catalytic activity of carbons for the dry reforming reaction. Oxidized carbons were found to be bad catalysts, especially under microwave heating. The importance of CO_2 reactivity for carbon

Research article ○ Abstract only

The comparison of particle oxidation and surface structure of diesel soot particles between fossil fuel and novel renewable diesel fuel

Matti Happonen, Tero Lähde, Maria E. Messing, Teemu Sarjovaara, … Jorma Keskinen
Pages 4008-4013

⬇ Purchase PDF   Article preview ∧

Abstract

Abstract

Conventional fossil diesel fuel and renewable diesel fuel based on hydrotreated vegetable oils (HVO) were compared regarding the oxidation characteristics of the generated soot particulate. The comparison was performed by utilizing a high-temperature oxidation tandem differential mobility analyser in which monodisperse soot aerosol was first selected and then heated in a high-temperature furnace. The particle size reduction caused by oxidation during the furnace treatment was then measured as a function of furnace temperature. The results indicate that soot oxidation is very similar between the studied fuels. This is supported by the obtained HR-TEM images and EELS-spectra which were practically indistinguishable between different fuels and engine conditions. The similar oxidation properties and surface structure between fossil and HVO-based

Research article ○ Abstract only

A comparison of injector flow and spray characteristics of biodiesel with petrodiesel

S. Som, D.E. Longman, A.I. Ramírez, S.K. Aggarwal
Pages 4014-4024

⬇ Purchase PDF   Article preview ∧

Abstract

Abstract

Performance and emission characteristics of compression ignition engines depend strongly on inner nozzle flow and spray behavior. These processes control the fuel air mixing, which in turn is critical for the combustion process. The differences in the physical properties of petrodiesel and biodiesel are expected to significantly alter the inner nozzle flow and spray structure and, thus, the performance and emission characteristics of the engine. In this study, the inner nozzle flow dynamics of these fuels are characterized by using the mixture-based cavitation model in FLUENT v6.3. Because of its lower vapor pressure, biodiesel was observed to cavitate less than petrodiesel. Higher viscosity of biodiesel resulted in loss of flow efficiency and reduction in injection velocity. Turbulence levels at the nozzle orifice exit were also lower for biodiesel. Using the recently

Research article ○ Abstract only

Experimental investigation of an industrial scale black liquor gasifier. 1. The effect of reactor operation parameters on product gas composition

Per Carlsson, Henrik Wiinikka, Magnus Marklund, Carola Grönberg, ... Rikard Gebart

Pages 4025-4034

⬇ Purchase PDF   Article preview ∧

Abstract

Abstract

A novel technology to mitigate the climate changes and improve energy security is Pressurized Entrained flow High Temperature Black Liquor Gasification (PEHT-BLG) in combination with an efficient fuel synthesis using the resulting syngas. In order to optimise the technology for use in a pulp and paper mill based biorefinery, it is of great importance to understand how the operational parameters of the gasifier affect the product gas composition. The present paper is based on experiments where gas samples were withdrawn from the hot part of a 3 MW entrained flow pressurized black liquor gasifier of semi industrial scale using a high temperature gas sampling system. Specifically, the influence of process conditions on product gas composition (CO_2, CO, H_2,

Research article ○ Abstract only

Optimization of pretreatment reaction for methyl ester production from chicken fat

Ertan Alptekin, Mustafa Canakci

Pages 4035-4039

⤓ Purchase PDF   Article preview ⌃

Abstract

Abstract

In biodiesel production, to use low cost feedstock such as rendered animal fats may reduce the biodiesel cost. One of the low cost animal fats is the chicken fat for biodiesel production. It is extracted from feather meal which is prepared from chicken wastes such as chicken feathers, blood, offal and trims after rendering process. However, chicken fats often contain significant amounts of FFA which cannot be converted to biodiesel using an alkaline catalyst due to the formation of soap. Therefore, the FFA level should be reduced to desired level (below 1%) by using acid catalyst before transesterification. For this aim, sulfuric, hydrochloric and sulfamic (amidosulfonic) acids were used for pretreatment reactions and the variables affecting the FFA level including alcohol molar ratio, acid catalyst amount and reaction time were investigated by using the chicken fat with

Research article ○ Abstract only

Ash deposition during the co-firing of bituminous coal with pine sawdust and olive stones in a laboratory furnace

P. Abreu, C. Casaca, M. Costa

Pages 4040-4048

⤓ Purchase PDF   Article preview ⌃

Abstract

Abstract

This article describes an experimental study on ash deposition during the co-firing of bituminous coal with pine sawdust and olive stones in a laboratory furnace. The main objective of this study was to relate the ash deposit rates with the type of biomass burned and its thermal percentage in

the blend. The thermal percentage of biomass in the blend was varied between 10% and 50% for both sawdust and olive stones. For comparison purposes, tests have also been performed using only coal or only biomass. During the tests, deposits were collected with the aid of an air-cooled deposition probe placed far from the flame region, where the mean gas temperature was around 640 °C. A number of deposit samples were subsequently analyzed on a scanning electron

Short Communications

Short communication ○ Abstract only

Bagasse from the mezcal industry as an alternative renewable energy produced in arid lands

L. Chávez-Guerrero, M. Hinojosa

Pages 4049-4052

⤓ Purchase PDF   Article preview ∧

Abstract

Abstract

In the mezcal industry, the xerophyte *Agave salmiana* is used to produce mezcal, and neither the plant nor its residues have been studied before as an alternative source of fuel. Bagasse and wasted fibers samples from alcoholic beverage production were collected in order to find out their properties as fuel. Another sample consists in pyrolyzed bagasse at 450 °C to produce carbon. DSC results revealed differences in the heat of combustion values, where pyrolyzed bagasse (19.36 MJ/kg) had a higher value than bagasse (9.55 MJ/kg) or the fiber (8.4 MJ/kg). SEM images showed the morphological changes in the fibers after their processing. TGA analysis showed the presence of different alcohols impregnated on the bagasse, which allows for an increase in heat of combustion. With these preliminary results it can be seen that it is possible to use the byproducts generated by

Short communication ○ Abstract only

Drag coefficient of Solid Recovered Fuels (SRF)

Gregory Dunnu, Jörg Maier, Uwe Schnell, Günter Scheffknecht

Pages 4053-4057

⤓ Purchase PDF   Article preview ⌄

Abstract

_____

Abstract

The numerical simulation of Solid Recovered Fuels (SRF) co-combustion in pulverised coal power plants requires a flexible particle model, which among other properties should be able to predict the aerodynamic behaviour of the irregular-shaped particles, especially their trajectories along the boiler axis. This will help to provide vital information on whether the SRF particles are entrained in the combustion gases or drop to the boiler bottom. One difficulty encountered in the process is the true value of the drag coefficient (C_D) of the coarse SRF particles. Most of the numerical simulation codes calculate the particle trajectories by integrating the force balance of the particles in which the C_D plays an important role. As a result, a true C_D of SRF will definitely lead to more realistic results.

Letters to the Editor

_____

Correspondence ○ No access

Photographic records of volatile release in the rapid heating of Victorian brown coals

J.C. Jones

Page 4058

⤓ Purchase PDF

Correspondence ○ No access

The composition of syngas from coal-biomass gasification

J.C. Jones

Page 4059

⤓ Purchase PDF

Correspondence ○ No access

Thermocouple signals from a fluidised bed reactor

J.C. Jones

Page 4060

⤓ **Purchase PDF**

Correspondence   ○   No access

The possible importance of solubility parameter in carbon dioxide sequestration in coal mines

J.C. Jones

Page 4061

⤓ **Purchase PDF**

‹ **Previous vol/issue**   **Next vol/issue** ›

About ScienceDirect

Remote access

Shopping cart

Advertise

Contact and support

Terms and conditions

Privacy policy

ℛ RELX™

Monodisperse monocomponent fuel droplet heating and evaporation

T. Kristyadi [a], V. Deprédurand [b], G. Castanet [b], F. Lemoine [b], S.S. Sazhin [c,*], A. Elwardany [c], E.M. Sazhina [c], M.R. Heikal [c]

[a] Mechanical Engineering Department, National Institute of Technology of Bandung, Jl PHH Mustofa No. 23, Bandung, Indonesia
[b] LEMTA, Nancy-Université, 2, Avenue de la Forêt de Haye, BP 160, 54504 Vandoeuvre-lès-Nancy, France
[c] Sir Harry Ricardo Laboratories, Centre for Automotive Engineering, School of Environment and Technology, Faculty of Science and Engineering, University of Brighton, Brighton BN2 4GJ, UK

ARTICLE INFO

ABSTRACT

The results of numerical and experimental studies of heating and evaporation of monodisperse acetone, ethanol, 3-pentanone, n-heptane, n-decane and n-dodecane droplets in an ambient air of fixed temperature and atmospheric pressure are reported. The numerical model took into account the finite thermal conductivity of droplets and recirculation inside them based on the effective thermal conductivity model and the analytical solution to the heat conduction equation inside droplets. The effects of interaction between droplets are taken into account based on the experimentally determined corrections to Nusselt and Sherwood numbers. It is pointed out that the interactions between droplets lead to noticeable reduction of their heating in the case of ethanol, 3-pentanone, n-heptane, n-decane and n-dodecane droplets, and reduction of their cooling in the case of acetone. Although the trends of experimentally observed droplet temperatures and radii are the same as predicted by the model taking into account the interaction between droplets, the actual values of the predicted droplet temperatures can differ from the observed ones by up to about 8 K, and the actual values of the predicted droplet radii can differ from the observed ones by up to about 2%. It is concluded that the effective thermal conductivity model, based on the analytical solution to the heat conduction equation inside droplets, can predict the observed average temperature of droplets with possible errors not exceeding several K, and observed droplet radii with possible errors not exceeding 2% in most cases. These results allow us to recommend the implementation of this model into CFD codes and to use it for multidimensional modelling of spray heating and evaporation based on these codes.

1. Introduction

The practical importance of accurate and computer efficient modelling of fuel droplet heating and evaporation in engineering applications is universally recognised (e.g. [1–3]). In most computational fluid dynamics (CFD) codes, this heating has been modelled assuming that there is no temperature gradient inside droplets (e.g. [4]). This assumption contradicts direct measurements of the temperature distribution inside droplets [5,6]. Bertoli and na Migliaccio [7] were perhaps the first to draw attention to the fact that taking into account the temperature gradient inside droplets can considerably increase the accuracy of the CFD modelling of combustion processes in Diesel engines. The analysis by these authors was based on the numerical solution of the heat conduction equation inside droplets. An alternative approach was suggested and developed in [8–13]. In these papers both finite liquid thermal conductivity and recirculation inside droplets (via the

effective thermal conductivity (ETC) model [14]) were taken into account by incorporating the analytical solution to the heat conduction equation inside the droplet into the numerical scheme. This approach was shown to be considerably more efficient (from the points of view of both accuracy and computer efficiency) than the one used in [7].

The preliminary validation of the model developed in [8–12] against published experimental data was reported in [9]. This validation, however, was limited to the comparison of predicted and calculated droplet diameters or global characteristics such as the ignition delay. A more direct validation of the model, based on the comparison of the predictions of the model and the results of simultaneous measurement of average temperatures and diameters of monodisperse monocomponent droplets, was reported in [6]. The latter comparison, however, was limited to just two substances: ethanol and acetone in two different experimental conditions. The aim of this paper is to perform a comparison between the predictions of the model and experimental data, similar to the one reported in [6] but for a wider range of substances and different experimental conditions. The substances to be considered

are: acetone, ethanol, 3-pentanone, n-heptane, n-decane and n-dodecane. The experimental data used in our analysis are the same as earlier reported in [15]. These data were used in [15] for validation of the model different from the one developed in [8–12] (see [16,17]). Hence, this paper is complementary to both earlier published papers [6,15].

The model used in our analysis is briefly summarised in Section 2. The formulae derived earlier will be simplified, where possible, and presented in the format actually used in the numerical code. The experimental setup is briefly described in Section 3. In Section 4 the predictions of the model are compared with experimental data. The main results of the paper are summarised in Section 5.

2. Model

In the case when the convection heat transfer coefficient $h(t) = h = \text{const}$, the solution of the transient heat conduction equation with $R_d = \text{const}$ and the corresponding boundary and initial conditions, applied to a small time step $\Delta t = t_1 - t_0$ gives the following value of temperature at the end of the time step t_1 [8]:

$$T(R, t_1) = \frac{R_d}{R} \sum_{n=1}^{\infty} \Lambda_n \sin(\lambda_n R/R_d) + T_{\text{eff}}(t_1), \qquad (1)$$

where:

$$\Lambda_n = \left[q_n - \frac{\mu_0(t_0) \sin \lambda_n}{\|v_n\|^2 \lambda_n^2} \right] \exp\left[-\kappa_0 \lambda_n^2 t_1 \right]$$
$$- \frac{\sin \lambda_n}{\kappa_0 \|v_n\|^2 \lambda_n^4} \frac{d\mu_0(t)}{dt} \bigg|_{t=t_0} \left(1 - \exp\left[-\kappa_0 \lambda_n^2 (t_1 - t_0) \right] \right), \qquad (2)$$

$$\mu_0(t) = \frac{h T_{\text{eff}}(t) R_d}{k_l}, \quad h_0 = (h R_d/k_l) - 1, \quad \|v_n\|^2 = \frac{1}{2}\left(1 + \frac{h_0}{h_0^2 + \lambda_n^2} \right),$$

$$\kappa_0 = \frac{k_l}{c_l \rho_l R_d^2}, \quad T_{\text{eff}} = T_g + \frac{\rho_l L \dot{R}_d}{h},$$

$$q_n = \frac{1}{\|v_n\|^2} \int_0^1 r T_0(r R_d) \sin(r \lambda_n) dr,$$

a set of positive eigenvalues λ_n numbered in ascending order ($n = 1, 2, \ldots$) is found from the solution of the following equation $\lambda \cos \lambda + h_0 \sin \lambda = 0$. If $T_0(R)$ is twice continuously differentiable, then the series in (1) converges absolutely and uniformly for all $t \geqslant 0$ and $R \in [0, R_d]$. When deriving (2) we assumed that the changes of $\frac{d\mu_0(t)}{dt}$ during the time step can be ignored. Ten terms in the series (1) were used in calculations. The effective thermal conductivity model was used in the case when the internal recirculation inside droplets is accounted [14]. The actual change of droplet radius is calculated as:

$$\dot{R}_d = \dot{R}_{dT} + \dot{R}_{dE}, \qquad (3)$$

where $\dot{R}_{dT}$ is the change of droplet radius due to thermal expansion. The value of $\dot{R}_{dE}$ is controlled by fuel vapour diffusion from the droplet surface. It can be found from equation [11]:

$$\dot{m}_d = 4\pi R_d^2 \dot{R}_{dE} \rho_l = -2\pi \bar{\rho}_g D_{Fa} R_d \text{Sh}_0 \ln(1 + B_M), \qquad (4)$$

where $\bar{\rho}_g$ is the average gas density (the contribution of fuel vapour to $\bar{\rho}_g$ has been ignored), D_{Fa} is the binary diffusion coefficient of fuel vapour in air (see [12]), $\text{Sh}_0 \equiv 2h_m R_d/D_{Fa}$ is the Sherwood number of non-evaporating droplets, h_m is the mass transfer coefficient. $B_M = (Y_{fs} - Y_\infty)/(1 - Y_{fs})$ is the Spalding mass transfer number, Y_{fs} and $Y_{f\infty}$ are the mass fractions of vapour near the droplet surface and at large distances from the droplet respectively. They are calculated from the Clausius–Clapeyron equation [19].

The Abramzon and Sirignano [14] model for the Sherwood and Nusselt numbers has been used. The values of the transport coefficients were taken for air at the temperature [11,18]: $T_{\text{ref}} = T_g + (T_g - T_s)/3$. The contribution of fuel vapour to the transport properties of air and the effects of droplets on air were ignored.

3. Experimental setup

Droplet diameters and average temperatures were measured using the experimental setup at the University of Nancy, which is described in a number of papers and theses, including [15–17]. This will be only briefly summarised below.

Linear monodisperse droplet streams are generated by Rayleigh disintegration of a liquid jet undergoing vibrations generated in a piezoelectric ceramic. The fuel is pre-heated in the injector by means of externally heated circulating water. The temperature of the fuel is measured exactly at the injection point with a K type thermocouple situated within the injector body. For specific frequencies of forced mechanical vibration, the liquid jet breaks up into equally spaced and monosized droplets. By adjusting the liquid flow rate and the piezoceramic frequency, it is possible to increase the droplet spacing up to about six times the droplet diameter. This, however, is accompanied by a modification of droplet sizes. The droplets are then injected into an enclosure fed with hot air coming from an electrical heater. In order to limit the thermal losses, a resistive electrical wire is inserted within the enclosure wall so that the wall temperature can be regulated to match that of the entering air. A temperature of up to 673 K could be reached. Destabilization of the droplet stream by the air motion can be a critical issue in this experiment. The air velocity is therefore maintained at between 0.1 and 0.3 m/s and the air flow is quietened by forcing it to go through a drilled wall and metallic foam. The problem of vapour saturation must be considered carefully due to the moderate movement of the air and the finite dimension of the chamber which has an inner diameter of 10 cm and a height of 14 cm. An estimate of the diffusion length L_d can be obtained considering diffusivity D_{Fa} is of the order of 10^{-5} m^2/s and maximal diffusion duration t is equal to 25 ms. The latter corresponds to the time required for a droplet to be transported through the enclosure. Based on these data we have $L_d = \sqrt{D_{Fa}t} \approx 0.5$ mm which is negligible compared to the inner radius of the enclosure. This ensures non-saturated conditions. Additionally, glass windows have been mounted in the wall to provide optical access. The two-colour laser-induced thermometry [20] is used to characterize the droplet temperature. The method involves the seeding of the liquid fuel with a small quantity of a fluorescent tracer, pyromethene 597-C8. The ratio of the fluorescence intensity detected on two spectral bands is a function of the temperature regardless of laser intensity, time-dependent tracer concentration, and measurement volume [21]. The velocity of the droplets is measured by Laser Doppler Velocimetry using the same laser light source as for the fluorescence excitation. The droplet size reduction is determined using the light scattering in the forward direction, where a stationary interference pattern is created. The measurement of the angular interfringe provides an accurate measurement of the droplet diameter.

Six liquid fuels were tested: acetone, ethanol, 3-pentanone, n-heptane, n-decane and n-dodecane. The approximations for the binary diffusion coefficients for each are given and discussed in Appendix A. Other physical properties of n-heptane and n-dodecane were assumed to be the same as in [12] (most of these properties were approximated using data from [22,23]). The physical properties of n-decane were taken to be the same as in [24], while the properties of acetone, ethanol and 3-pentanone were taken from [17,22,25].

An investigation of a number of droplet streams was performed. The temperature, velocity and diameter of the droplets were measured simultaneously at each measurement point. The periodicity of the droplets in the chain and the steady-state nature of their stream allowed us to convert the droplet distance from the injector into time. In our analysis, we focused on the evolution of droplets' temperatures and radii, starting from the moment when the first droplet was observed near the entrance to the enclosure. By placing a thermocouple at different locations it was established that air temperature T_a did not vary inside the chamber. Hence, it was considered to be constant during each experiment in our modelling. The droplet absolute velocities were approximated as linear functions of time (measured from the moment of injection):

$$v_d = v_1 - v_2 t, \qquad (5)$$

where constants v_1 and v_2 were determined for each experiment, alongside the ratios $\mathrm{Nu}_n = \mathrm{Nu}/\mathrm{Nu}_{iso}$ and $\mathrm{Sh}_n = \mathrm{Sh}/\mathrm{Sh}_{iso}$, describing the effects of interaction between droplets in the stream, where the subscript $_{iso}$ refers to isolated droplets. The error of determination of v_d is comparable with the ambient air velocities up to 0.3 m/s. This justifies our assumption that the absolute droplet velocities, estimated by Eq. (5), are equal to droplet velocities relative to ambient air. These velocities are used for the estimation of the Nusselt and Sherwood numbers for isolated droplets.

The values of the Nusselt and Sherwood numbers were estimated based on simultaneous measurements of droplet sizes and mean temperatures. These measurements allowed us to evaluate heat fluxes responsible for droplet heating and evaporation rates. These rates, alongside the measured time evolution of droplet mean temperatures, were used for the estimate of the convective heat flux, responsible for droplet heating, and mass flux of fuel vapour leaving the droplet. The main difficulty in converting these estimates into the estimates of the Nusselt and Sherwood numbers relates to the fact that the surface droplet temperatures T_s were not directly measured and had to be estimated. This issue is addressed in [15,17], where an iterative approach based on a simplified analysis of the energy balance of evaporation was used. After the droplet surface temperatures were estimated, the values of

the Nusselt and Sherwood numbers were derived from the estimated heat and mass fluxes. Using the values of these numbers for isolated droplets, calculated from the Abramzon and Sirignano [14] model, the values of Nu_n and Sh_n, presented in Table 1, were calculated.

Three experiments were performed with each fuel, except 3-pentanone, for which only two experiments were performed. The values of T_a, distance parameter C (ratio of the distance between droplets and their diameters), initial droplet diameters D_{d0} (measured directly when the first droplets near the entrance to the enclosure were observed), Nu_n, Sh_n, v_1 and v_2 for each experiment are presented in Table 1, alongside boiling and critical temperatures (T_b and T_c) for each substance [22]. The values of C are shown to indicate the closeness of droplets in our experiments. In contrast to [6] they were not used to estimate Nusselt and Sherwood numbers.

The uncertainties in the measurement of the droplet diameters are expected to be about ±0.5 μm in most cases and the uncertainties in the temperature measurements are expected to be about ±1 K. Depending on the fuel and the experimental conditions, the uncertainties in the estimates of Sh_n and Nu_n are expected to be between 2% and 25% [15]. However, in the case of *n*-decane and *n*-dodecane, which have particularly low volatility, the mass loss due to evaporation was so low that it was not possible to determine accurately a value for Sh_n. Therefore, for these cases, the values of Sh_n were not estimated experimentally and we assumed them to be equal to Nu_n.

4. Results

The plots of temperature versus time for Case 1 for acetone and *n*-heptane, calculated using our model and obtained in the experiment are shown in Figs. 1 and 2. The values of parameters shown in Table 1 were used in calculations. The calculations were performed ignoring the interactions between droplets (indicated by subscript $_{iso}$) and taking them into account, based on the values of Sh_n and Nu_n given in Table 1. Time in all figures is measured from the moment of injection.

Table 1
The values of T_a, C, D_{d0}, Nu_n, Sh_n, v_1 and v_2 for three experiments with acetone, ethanol, 3-pentanone, *n*-heptane, *n*-decane and *n*-dodecane droplets (abbreviated as acet, ethan, 3-pen, *n*-hep, *n*-dec and *n*-dod). The droplet velocities in m/s are approximated as $v_d = v_1 - v_2 t$, where t is in ms. In the case of *n*-decane and *n*-dodecane, the values of Sh_n were not estimated experimentally, but assumed to be equal to Nu_n.

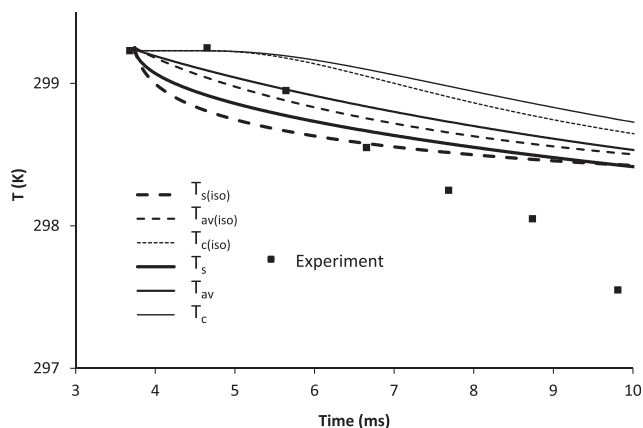| Case	Parameter	Acet	Ethan	3-Pen	*n*-Hep	*n*-Dec	*n*-Dod
	T_b (K)	329.22	351.80	375.14	371.57	477.30	489.48
	T_c (K)	508.10	513.92	561.50	540.20	617.70	658.00
1	T_a (K)	640	643	634	644	643	643
1	C	4.5	4.3	4.9	4.4	3.7	4.6
1	D_{d0} (μm)	122.6	119.6	118.2	131.1	121.5	110.0
1	Nu_n	0.42	0.26	0.23	0.38	0.18	0.19
1	Sh_n	0.43	0.38	0.53	0.57	0.18	0.19
1	v_1 (m/s)	11.16	9.869	10.86	12.8	9.59	9.246
1	v_2 (m/(s · ms))	0.198	0.214	0.254	0.329	0.220	0.281
2	T_a (K)	645	643	645	645	645	644
2	C	5.5	6.1	4.0	5.3	4.4	6.9
2	D_{d0} (μm)	132.2	130.28	123.3	134.2	128.37	129.0
2	Nu_n	0.43	0.42	0.22	0.35	0.24	0.22
2	Sh_n	0.42	0.82	0.33	0.84	0.24	0.22
2	v_1 (m/s)	14.12	12.64	9.454	15.44	11.88	13.14
2	v_2 (m/(s · ms))	0.276	0.268	0.224	0.446	0.329	0.573
3	T_a (K)	647	644	n/a	647	647	643
3	C	3.3	3.1	n/a	3.8	5.4	3.0
3	D_{d0} (μm)	107.2	112.4	n/a	122.8	124.8	98.99
3	Nu_n	0.35	0.36	n/a	0.28	0.18	0.22
3	Sh_n	0.26	0.38	n/a	0.50	0.18	0.22
3	v_1 (m/s)	7.122	6.889	n/a	10.56	13.55	6.091
3	v_2 (m/(s · ms))	0.113	0.123	n/a	0.244	0.307	0.218

Fig. 1. Plots of the time evolution of the experimentally observed temperatures of acetone droplets for Case 1, and temperatures at the surface of these droplets (T_s), average temperatures in the droplets (T_{av}) and the temperatures at the centre of the droplets (T_c), predicted by the models ignoring the interactions between droplets (indicated by the subscript $_{iso}$), and taking into account these interactions. The input parameters of the models were taken from Table 1.
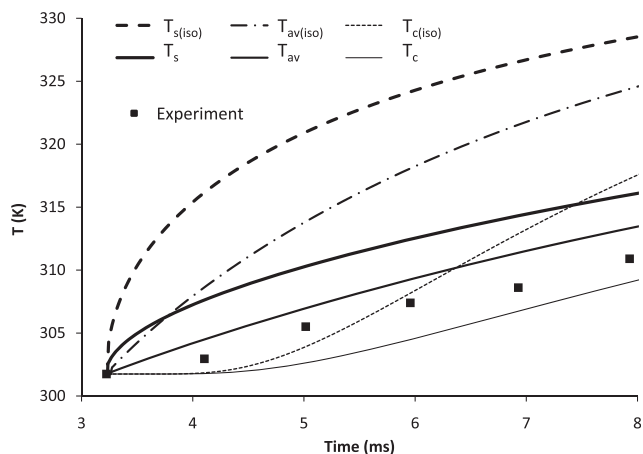

Fig. 2. The same as Fig. 1 but for n-heptane droplets.

The calculations started at the time when the droplets were first observed near the entrance to the chamber. The observed temperatures and radii of these droplets were used as the initial temperatures and radii in the model. It was assumed that initially there was no temperature gradient inside droplets.

As follows from Figs. 1 and 2, the plots referring to interacting and non-interacting (isolated) droplets are noticeably different for both substances. Similarly, the plots referring to the temperatures at the centres of the droplets, average temperatures, and the temperatures at the surfaces of the droplets are well separated. This result is similar to the one reported in [6], and it shows the limitation of the assumption, which is widely used in CFD codes, that the gradient of temperature inside droplets can be ignored.

The observed temperatures of acetone droplets, shown in Fig. 1, look rather different from the ones predicted by the model. Note, however, that the difference between the average temperature, predicted by the model, taking into account the interaction between droplets (T_{av}), and the experimentally observed temperatures is always less than 1 K, and can be naturally attributed to the uncertainty of the measurements, and uncertainties of the input parameters used in calculations.

In the case of n-heptane and n-dodecane droplets, the closeness between the experimentally observed temperatures and T_{av} was

the most visible, compared with other droplets. The best matching between the experimentally observed temperatures and T_{av} can be seen for n-heptane, as shown in Fig. 2. However, even in this case, the actual deviation between these temperatures sometimes exceeds 1 K. This means that the model cannot predict the observed average droplet temperatures with errors less than about 1 K. For both these substances, the experimentally observed temperatures always lie between the temperatures T_s and T_c, predicted by the model, taking into account the interaction between droplets.

In the case of ethanol droplets the experimentally observed temperatures were closer to the ones predicted by the model, taking into account the interaction between droplets, than the one ignoring this interaction. However, the deviation between the experimental points and T_{av} for these droplets (up to about 3 K) was larger than in the case of acetone, n-heptane and n-dodecane droplets. The temperatures for 3-pentanone and n-decane were generally similar to those for ethanol, with the maximal deviation between the experimental points and T_{av} about 3 K for 3-pentanone and about 6 K for n-decane.

The plots of normalised droplet radii R_d/R_{d0} versus time for Case 1 for all six substances, calculated using our model and obtained in the experiment, are shown in Figs. 3 and 4. The initial values of droplet radii were taken to be equal to those for the droplets for which the first measurements of droplet temperature were taken.

When calculating the time evolution of R_d, both droplet evaporation and thermal expansion were taken into account based on Eq.
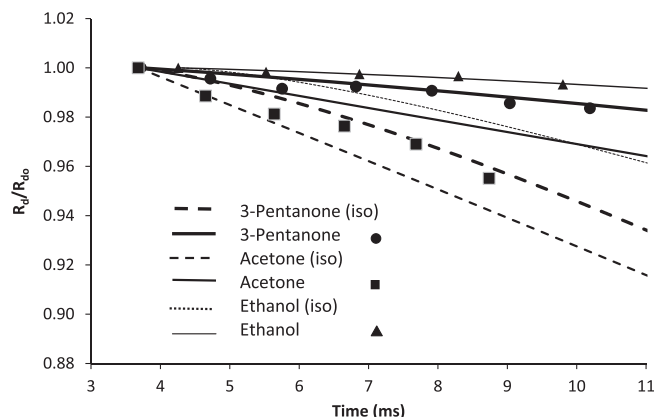

Fig. 3. Plots of the time evolution of the experimentally observed and modelled normalised droplet radii R_d/R_{d0} for acetone, ethanol and 3-pentanone droplets for Case 1. Models ignoring the interactions between droplets (indicated by the subscript $_{iso}$), and taking into account these interactions, were used. The input parameters of the models were taken from Table 1.

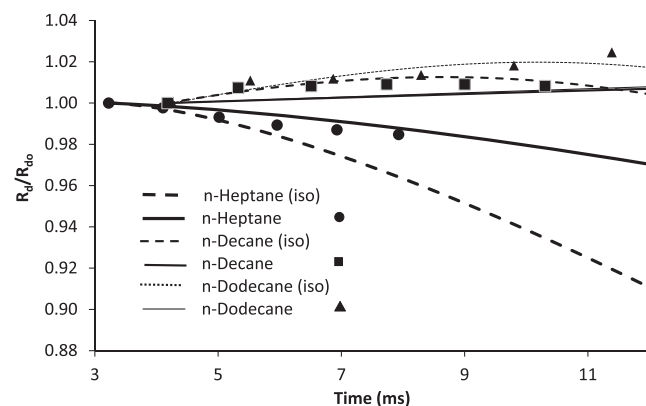**Fig. 4.** The same as Fig. 3 but for n-heptane, n-decane and n-dodecane droplets.

(3). The values of parameters used for these calculations are given in Table 1. As follows from these figures, the plots referring to interacting and non-interacting droplets are noticeably different for all substances, as for the temperature plots shown in Figs. 1 and 2. Note that in contrast to [15] we presented the plots of the ratios of radii rather than the ratios of radii squared. The latter would have been justified if the analysis had been focused on droplet evaporation beyond the heat-up period, when the d^2-law is valid. In our case, however, the focus is on the heat-up period itself (cf. [26]).

As follows from Figs. 3 and 4, the effects of interaction between droplets lead to a decrease in the rate of reduction of their radii in the case of acetone, ethanol, 3-pentanone and n-heptane, but to a slowing down of the increase of these radii in the case of n-decane and n-dodecane. In the latter case, the effect of the thermal expansion of droplets dominates over the effects of evaporation. In the case of ethanol, 3-pentanone, n-heptane and n-decane the agreement between experimental plots and predictions of the model, taking into account the interaction between droplets, looks almost ideal. However, for acetone and n-dodecane the experimental data lie between the predictions of the models ignoring the interaction between droplets and taking them into account. Even in the case of these two substances, the deviation between the experimental results and the predictions of the model, taking into account the interaction between droplets, does not exceed about 2%.

For the results referring to Cases 2 and 3 we restricted our analysis to comparison of the experimental data with the average temperatures and R_d/R_{d0} predicted by the model taking into account the interaction between droplets, as was done in [15]. Instead of the actual droplet average temperatures T, studied for Case 1, the analysis for Cases 2 and 3 is focused on the difference between these temperatures and the initial droplet temperatures T_0. The corresponding plots for $T - T_0$ versus time for Case 2 for all six substances are shown in Fig. 5. As follows from this figure, although the trends predicted by the model are similar to the ones observed experimentally, there are noticeable deviations between the actual values of predicted and observed average droplet temperatures. The maximal deviation between them is seen for n-decane and n-dodecane droplets. The minimal deviation between them is seen for 3-pentanone droplets.

The plots of R_d/R_{d0} versus time for Case 2 for the same substances as in Fig. 5, are shown in Fig. 6. As one can see from this figure, the trends predicted by the model are similar to the ones
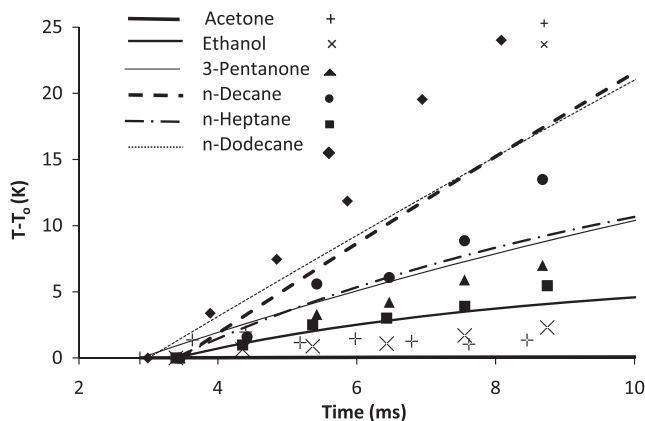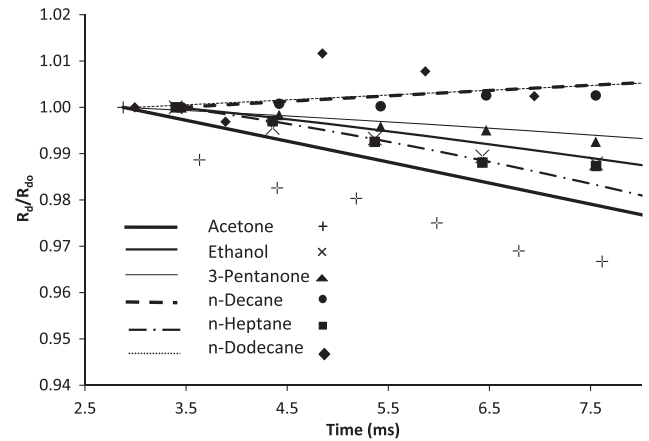

Fig. 6. The same as Fig. 5 but for R_d/R_{d0}.

observed experimentally, but there are noticeable deviations between the observed and predicted values of this ratio, as in the case of Fig. 5. The maximal deviation between these ratios (up to almost 2%) is seen for acetone droplets. The minimal deviation between these ratios is seen for 3-pentanone droplets. Hence, for Case 2 the best agreement between experimental and modelled results for both temperatures and radii is observed for 3-pentanone droplets.

The plots for $T - T_0$ versus time for Case 3 for acetone, ethanol, n-heptane, n-decane and n-dodecane (there is no data for 3-pentanone for Case 3) are shown in Fig. 7. As one can see from this figure, the agreement between experimental and modelled results is very good for acetone, while the deviation between the experimentally observed temperatures and those predicted by the model could reach more than about 5 K for ethanol and n-dodecane (although the observed and predicted trends for both substances are the same). The plots of R_d/R_{d0} versus time for Case 3 for the same substances as in Fig. 7, are shown in Fig. 8. As can be seen from this figure, the best agreement between experimental and modelled results can be seen for n-decane and n-heptane, and the worst for acetone and n-dodecane. However, even in the case of acetone and n-dodecane, both experimental and modelled results show the same trends and the deviation between them does not exceed 2%.

Several factors are expected to contribute to the difference between the modelled results presented in this paper and ones reported in [15,17]. Some approximations for transport coefficients used in this paper are different from those used in [15,17]. We used the time-averaged values of Nu_n and Sh_n, while both these parameters varied with time.
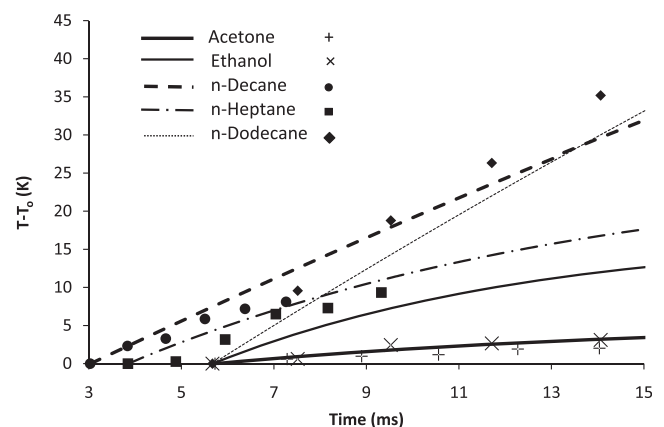

Fig. 5. Plots of the time evolution of the experimentally observed droplet temperatures $T - T_0$, where T_0 are the initial droplet temperatures, and the average temperatures of droplets, predicted by the model taking into account the interaction between droplets. The results for acetone, ethanol, 3-pentanone, n-heptane, n-decane and n-dodecane droplets for Case 2 are shown. The input parameters of the models were taken from Table 1.

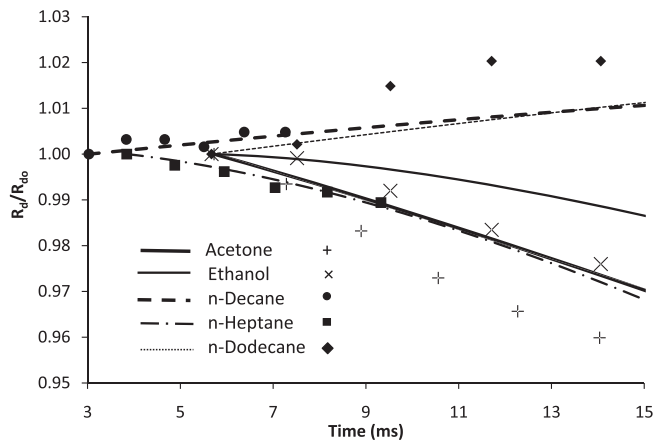**Fig. 7.** The same as Fig. 5 but for Case 3, except without the results for n-pentanone.

Fig. 8. The same as Fig. 7 but for R_d/R_{d0}.

5. Conclusions

Heating and evaporation of monodisperse acetone, ethanol, 3-pentanone, n-heptane, n-decane and n-dodecane droplets in ambient air at fixed temperature and atmospheric pressure have been studied numerically and experimentally. Droplet initial diameters varied from 99 to 135 μm, while ambient air temperatures varied from 634 to 647 K. The numerical model took into account the finite thermal conductivity of droplets and recirculation inside them based on the effective thermal conductivity model and the analytical solution to the heat conduction equation inside droplets. The initial values of droplet temperatures and radii were assumed to be equal to those observed experimentally for the first recorded droplet. It was assumed that initially there was no temperature gradient inside droplets.

It is pointed out that the interactions between droplets lead to noticeable reduction of their heating in the case of ethanol, 3-pentanone, n-heptane, n-decane and n-dodecane droplets, and enhancement of their cooling in the case of acetone. The interaction between droplets leads to a decrease in the rate of reduction of their radii in the case of acetone, ethanol, 3-pentanone and n-heptane, but to a slowing down of the increase of these radii in the case of n-decane and n-dodecane. In the latter case, the effect of the thermal expansion of droplets dominates over the effects of evaporation.

Although the trends of experimentally observed droplet temperatures and radii are the same as predicted by the model taking into account the interaction between droplets, the values of the predicted droplet temperatures can differ from the observed ones by up to about 8 K, and the actual values of the predicted droplet radii can differ from the observed ones by up to about 2%.

Combining the above results and those reported previously in [6] we can conclude that the effective thermal conductivity model, based on the analytical solution to the heat conduction equation inside droplets, can predict the observed average temperature of droplets with possible errors not exceeding several K, and observed droplet radii with possible errors not exceeding 2% in most cases. These results confirm our previous conclusion (see [9,10,12]) that this model can be recommended for implementation in CFD codes and used for multidimensional modelling of spray heating and evaporation based on these codes.

Appendix A. Binary diffusion coefficient for fuel vapour

The binary diffusion coefficient for all fuels was estimated using the following equation [27]:

$$D_{Fa} = 1.8583 \times 10^{-7} \sqrt{T^3 \left(\frac{1}{M_F} + \frac{1}{M_a}\right)} \frac{1}{p\sigma_{Fa}^2 \Omega_{Fa}(T^*)}, \qquad (A1)$$

where D_{Fa} is in m²/s, p is in atm (1 atm = 0.101 MPa), T is in K, $\sigma_{Fa} = 0.5(\sigma_F + \sigma_a)$ is the minimal distance between molecules in Angström, Ω_{Fa} is the collision integral, the value of which depends on the normalised temperature $T^* = Tk_B/\epsilon$, k_B is the Boltzmann constant, $\epsilon = \sqrt{\epsilon_F \epsilon_a}$; the subscript $_a$ indicates air. Note that the formula for the binary diffusion coefficient used in [22] differs from the one presented above in terms of the value of the coefficient (they used 1.8623 instead of 1.8583). The difference between the values of this coefficient predicted by two formulae (0.2%) can be safely ignored in most practical applications. Note that there is a typo in Eq. (B5) of [12]. $\sigma_a = 3.617$ Angström, $\epsilon_a/k_B = 97.0$ K (Table E.1 in [27]). The values of these parameters and molar masses for acetone, ethanol, n-heptane, 3-pentanone and n-dodecane are given in Table A1.

There is some controversy regarding the values of σ_F and ϵ_F/k_B for n-heptane and n-dodecane. We used the data leading to the best fit with experimental data. These are indicated by * in the ϵ_F/k_B column.

Once the value of T^* had been found, the collision integral Ω_{Fa} could be obtained from Table E.2 [27]. However, we found it more convenient to use the analytical approximation of Ω_{Fa} given by Eq. (E.2-2) of [27]).

For the binary diffusion coefficient of n-decane ($C_{10}H_{22}$) we used the following approximation [24]:

$$D_{Fa} = 5.46 \times 10^{-6} \frac{1}{1.01p} \left(\frac{T}{300}\right), \qquad (A2)$$

where p is in atm, as in Eq. (A1).

Table A1
The values of σ_F, ϵ_F/k_B and molar masses for acetone, ethanol, n-heptane, 3-pentanone and n-dodecane, as inferred from various sources.

Fuel	Reference	Formula	σ_F in Angström	ϵ_F/k_B in K	Molar mass in kg/kmole
Acetone	[22]	C_3H_6O	4.600	560.2	58.080
Ethanol	[22]	C_2H_6O	4.530	362.6	46.069
n-Heptane	[28,22]	C_7H_{16}	5.949	399.3*	100.204
n-Heptane	[27]	C_7H_{16}	6.663	352	100.20
n-Heptane	[29,22]	C_7H_{16}	6.498	455.04	46.069
3-Pentanone	[28,22]	$C_5H_{10}O$	4.22	351.562	86.134
n-Dodecane	[28,22]	$C_{12}H_{26}$	9.37	245.0	170.338
n-Dodecane	[29,22]	$C_{12}H_{26}$	6.5972	454.6768*	170.338

Data indicated by * in the ϵ_F/k_B column were used in our analysis.

References

[1] Polyanin AD, Kutepov AM, Vyazmin AV, Kazenin DA. Hydrodynamics mass and heat transfer in chemical engineering. London and New York: Taylor and Francis; 2002.

[2] Michaelides EE. Particles, bubbles and drops. Singapore: World Scientific; 2006.

[3] Faghri A, Zhang Y. Transport phenomena in multiphase systems. Burlington: Elsevier; 2006.

[4] Sazhina EM, Sazhin SS, Heikal MR, Babushok VI, Johns R. A detailed modelling of the spray ignition process in diesel engines. Combust Sci Technol 2000;160:317–44.

[5] Castanet G, Lebouché M, Lemoine F. Heat and mass transfer of combusting monodisperse droplets in a linear stream. Int J Heat Mass Trans 2005;48:3261–75.

[6] Maqua C, Castanet G, Grisch F, Lemoine F, Kristyadi T, Sazhin SS. Monodisperse droplet heating and evaporation: experimental study and modelling. Int J Heat Mass Trans 2008;51:3932–45.

[7] Bertoli C, na Migliaccio M. A finite conductivity model for diesel spray evaporation computations. Int J Heat Fluid Flow 1999;20:552–61.

[8] Sazhin SS, Krutitskii PA, Abdelghaffar WA, Sazhina EM, Mikhalovsky SV, Meikle ST, et al. Transient heating of diesel fuel droplets. Int J Heat Mass Trans 2004;47:3327–40.

[9] Sazhin SS, Abdelghaffar WA, Sazhina EM, Heikal MR. Models for droplet transient heating: effects on droplet evaporation, ignition, and break-up. Int J Therm Sci 2005;44:610–22.

[10] Sazhin SS, Abdelghaffar WA, Krutitskii PA, Sazhina EM, Heikal MR. New approaches to numerical modelling of droplet transient heating and evaporation. Int J Heat Mass Trans 2005;48:4215–28.

[11] Sazhin SS. Advanced models of fuel droplet heating and evaporation. Prog Energy Combust Sci 2006;32:162–214.

[12] Sazhin SS, Kristyadi T, Abdelghaffar WA, Heikal MR. Models for fuel droplet heating and evaporation: comparative analysis. Fuel 2006;85: 1613–30.

[13] Sazhin SS, Krutitskii PA, Martynov SB, Mason D, Heikal MR, Sazhina EM. Transient heating of a semitransparent spherical body. Int J Therm Sci 2007;46:444–57.

[14] Abramzon B, Sirignano WA. Droplet vaporization model for spray combustion calculations. Int J Heat Mass Trans 1989;32:1605–18.

[15] Deprédurand V, Castanet G, Lemoine F. Heat and mass transfer in evaporating droplets in interaction: influence of the fuel. Int J Heat Mass Trans 2010;53:3495–502.

[16] Castanet G. Etude aérothermique d'un jet de gouttes monodispersé en évaporation et en combustion à l'aide de méthodes optiques. Thèse présentée pour l'obtention du grade de Docteur de l'Université Henri Poincaré, Vandoeuvre-Les-Nancy; 2004.

[17] Deprédurand V. Approche experimentale de l' évaporation de sprays de combustibles multicomposants. Thèse présentée pour l'obtention du grade de Docteur de l'Institut National Polytechnique de Lorraine, Vandoeuvre-Les-Nancy; 2009.

[18] Incropera FP, DeWitt DP. Fundamentals of heat and mass transfer. 5th ed. John Wiley and Sons; 2002.

[19] Kuo KK. Principles of combustion. John Wiley and Sons; 1986.

[20] Lavieille P, Lemoine F, Lavergne G, Lebouché M. Evaporating and combusting droplet temperature measurements using two color laser induced fluorescence. Exp Fluids 2001;31:45–55.

[21] Deprédurand V, Miron P, Labergue A, Wolff M, Castanet G, Lemoine F. A temperature sensitive tracer suitable for two-colour laser-induced fluorescence thermometry applied to evaporating droplets. Measur Sci Technol 2008;19(10):1–12.

[22] Poling BE, Prausnitz JM, O'Connell J. The properties of gases and liquids. New York: McGraw-Hill; 2000.

[23] Maxwell JB. Data book on hydrocarbons: application to process engineering. New York: Van Nostrand Company, Inc.; 1950.

[24] Abramzon B, Sazhin S. Convective vaporization of fuel droplets with thermal radiation absorption. Fuel 2006;85:32–46.

[25] National Institute of Standards and Technology (NIST). Chemistry WebBook, 2010. <http://webbook.nist.gov/chemistry/>.

[26] Sazhin SS, Krutitskii PA, Gusev IG, Heikal M. Transient heating of an evaporating droplet. Int J Heat Mass Trans 2010;53:2826–36.

[27] Bird RB, Stewart EW, Lightfoot EN. Transport phenomena. 2nd ed. New York, Chichester: Wiley and Sons; 2002.

[28] Hirschfelder JO, Curtiss CF, Bird RB. Molecular theory of gases and liquids. 4th ed. New York, Chichester: John Wiley and Sons; 1967.

[29] Paredes MLL, Nobrega R, Tavares FW. A completely analytical equation of state for mixture of square-well chain fluid of variable well width. In: XIX Inter American Congress of Chemical Engineering, Agios de Sao Pedro, Brazil; 24–27 September 2000 [paper no. 396].

Monodisperse monocomponent fuel droplet heating and evaporation

By Kristyadi MS

Monodisperse monocomponent fuel droplet heating and evaporation

T. Kristyadi [a], V. Deprédurand [b], G. Castanet [b], F. Lemoine [b], S.S. Sazhin [c,*], A. Elwardany [c], E.M. Sazhina [c], M.R. Heikal [c]

[a] Mechanical Engineering Department, National Institute of Technology of Bandung, Jl PHH Mustofa No. 23, Bandung, Indonesia
[b] LEMTA, Nancy-Université, 2, Avenue de la Forêt de Haye, BP 160, 54504 Vandoeuvre-lès-Nancy, France
[c] Sir Harry Ricardo Laboratories, Centre for Automotive Engineering, School of Environment and Technology, Faculty of Science and Engineering, University of Brighton, Brighton BN2 4GJ, UK

ARTICLE INFO

ABSTRACT

The results of numerical and experimental studies of heating and evaporation of monodisperse acetone, ethanol, 3-pentanone, n-heptane, n-decane and n-dodecane droplets in an ambient air of fixed temperature and atmospheric pressure are reported. The numerical model took into account the finite thermal conductivity of droplets and recirculation inside them based on the effective thermal conductivity model and the analytical solution to the heat conduction equation inside droplets. The effects of interaction between droplets are taken into account based on the experimentally determined corrections to Nusselt and Sherwood numbers. It is pointed out that the interactions between droplets lead to noticeable reduction of their heating in the case of ethanol, 3-pentanone, n-heptane, n-decane and n-dodecane droplets, and reduction of their cooling in the case of acetone. Although the trends of experimentally observed droplet temperatures and radii are the same as predicted by the model taking into account the interaction between droplets, the actual values of the predicted droplet temperatures can differ from the observed ones by up to about 8 K, and the actual values of the predicted droplet radii can differ from the observed ones by up to about 2%. It is concluded that the effective thermal conductivity model, based on the analytical solution to the heat conduction equation inside droplets, can predict the observed average temperature of droplets with possible errors not exceeding several K, and observed droplet radii with possible errors not exceeding 2% in most cases. These results allow us to recommend the implementation of this model into CFD codes and to use it for multidimensional modelling of spray heating and evaporation based on these codes.

Crown Copyright © 2010 Published by Elsevier Ltd. All rights reserved.

1. Introduction

The practical importance of accurate and computer efficient modelling of fuel droplet heating and evaporation in engineering applications is universally recognised (e.g. [1–3]). In most computational fluid dynamics (CFD) codes, this heating has been modelled assuming that there is no temperature gradient inside droplets (e.g. [4]). This assumption contradicts direct measurements of the temperature distribution inside droplets [5,6]. Bertoli and na Migliaccio [7] were perhaps the first to draw attention to the fact that taking into account the temperature gradient inside droplets can considerably increase the accuracy of the CFD modelling of combustion processes in Diesel engines. The analysis by these authors was based on the numerical solution of the heat conduction equation inside droplets. An alternative approach was suggested and developed in [8–13]. In these papers both finite liquid thermal conductivity and recirculation inside droplets (via the

effective thermal conductivity (ETC) model [14]) were taken into account by incorporating the analytical solution to the heat conduction equation inside the droplet into the numerical scheme. This approach was shown to be considerably more efficient (from the points of view of both accuracy and computer efficiency) than the one used in [7].

The preliminary validation of the model developed in [8–12] against published experimental data was reported in [9]. This validation, however, was limited to the comparison of predicted and calculated droplet diameters or global characteristics such as the ignition delay. A more direct validation of the model, based on the comparison of the predictions of the model and the results of simultaneous measurement of average temperatures and diameters of monodisperse monocomponent droplets, was reported in [6]. The latter comparison, however, was limited to just two substances: ethanol and acetone in two different experimental conditions. The aim of this paper is to perform a comparison between the predictions of the model and experimental data, similar to the one reported in [6] but for a wider range of substances and different experimental conditions. The substances to be considered

---

* Corresponding author. Tel.: +44 1273 642677; fax: +44 1273 642301.
E-mail address: S.Sazhin@brighton.ac.uk (S.S. Sazhin).

are: acetone, ethanol, 3-pentanone, n-heptane, n-decane and n-dodecane. The experimental data used in our analysis are the same as earlier reported in [15]. These data were used in [15] for validation of the model different from the one developed in [8–12] (see [16,17]). Hence, this paper is complementary to both earlier published papers [6,15].

The model used in our analysis is briefly summarised in Section 2. The formulae derived earlier will be simplified, where possible, and presented in the format actually used in the numerical code. The experimental setup is briefly described in Section 3. In Section 4 the predictions of the model are compared with experimental data. The main results of the paper are summarised in Section 5.

2. Model

In the case when the convection heat transfer coefficient $h(t) = h = \text{const}$, the solution of the transient heat conduction equation with $R_d = \text{const}$ and the corresponding boundary and initial conditions, applied to a small time step $\Delta t = t_1 - t_0$ gives the following value of temperature at the end of the time step t_1 [8]:

$$T(R, t_1) = \frac{R_d}{R} \sum_{n=1}^{\infty} \Lambda_n \sin(\lambda_n R/R_d) + T_{\text{eff}}(t_1), \tag{1}$$

where:

$$\Lambda_n = \left[q_n - \frac{\mu_0(t_0) \sin \lambda_n}{\|v_n\|^2 \lambda_n^2} \right] \exp\left[-\kappa_0 \lambda_n^2 t_1\right]$$

$$- \frac{\sin \lambda_n}{\kappa_0 \|v_n\|^2 \lambda_n^4} \frac{d\mu_0(t)}{dt}\bigg|_{t=t_0} \left(1 - \exp\left[-\kappa_0 \lambda_n^2 (t_1 - t_0)\right]\right), \tag{2}$$

$$\mu_0(t) = \frac{hT_{\text{eff}}(t)R_d}{k_l}, \quad h_0 = (hR_d/k_l) - 1, \quad \|v_n\|^2 = \frac{1}{2}\left(1 + \frac{h_0}{h_0^2 + \lambda_n^2}\right),$$

$$\kappa_0 = \frac{k_l}{c_l \rho_l R_d^2}, \quad T_{\text{eff}} = T_g + \frac{\rho_l L \dot{R}_d}{h},$$

$$q_n = \frac{1}{\|v_n\|^2} \int_0^1 r T_0(r R_d) \sin(r \lambda_n) dr,$$

a set of positive eigenvalues λ_n numbered in ascending order $(n = 1, 2, \ldots)$ is found from the solution of the following equation $\lambda \cos \lambda + h_0 \sin \lambda = 0$. If $T_0(R)$ is twice continuously differentiable, then the series in (1) converges absolutely and uniformly for all $t \geqslant 0$ and $R \in [0, R_d]$. When deriving (2) we assumed that the changes of $\frac{d\mu_0(t)}{dt}$ during the time step can be ignored. Ten terms in the series (1) were used in calculations. The effective thermal conductivity model was used in the case when the internal recirculation inside droplets is accounted [14]. The actual change of droplet radius is calculated as:

$$\dot{R}_d = \dot{R}_{dT} + \dot{R}_{dE}, \tag{3}$$

where $\dot{R}_{dT}$ is the change of droplet radius due to thermal expansion. The value of $\dot{R}_{dE}$ is controlled by fuel vapour diffusion from the droplet surface. It can be found from equation [11]:

$$\dot{m}_d = 4\pi R_d^2 \dot{R}_{dE} \rho_l = -2\pi \bar{\rho}_g D_{Fa} R_d \text{Sh}_0 \ln(1 + B_M), \tag{4}$$

where $\bar{\rho}_g$ is the average gas density (the contribution of fuel vapour to $\bar{\rho}_g$ has been ignored), D_{Fa} is the binary diffusion coefficient of fuel vapour in air (see [12]), $\text{Sh}_0 \equiv 2h_m R_d/D_{Fa}$ is the Sherwood number of non-evaporating droplets, h_m is the mass transfer coefficient. $B_M = (Y_{fs} - Y_{f\infty})/(1 - Y_{fs})$ is the Spalding mass transfer number, Y_{fs} and $Y_{f\infty}$ are the mass fractions of vapour near the droplet surface and at large distances from the droplet respectively. They are calculated from the Clausius–Clapeyron equation [19].

The Abramzon and Sirignano [14] model for the Sherwood and Nusselt numbers has been used. The values of the transport coefficients were taken for air at the temperature [11,18]: $T_{\text{ref}} = T_g + (T_g - T_s)/3$. The contribution of fuel vapour to the transport properties of air and the effects of droplets on air were ignored.

3. Experimental setup

Droplet diameters and average temperatures were measured using the experimental setup at the University of Nancy, which is described in a number of papers and theses, including [15–17]. This will be only briefly summarised below.

Linear monodisperse droplet streams are generated by Rayleigh disintegration of a liquid jet undergoing vibrations generated in a piezoelectric ceramic. The fuel is pre-heated in the injector by means of externally heated circulating water. The temperature of the fuel is measured exactly at the injection point with a K type thermocouple situated within the injector body. For specific frequencies of forced mechanical vibration, the liquid jet breaks up into equally spaced and monosized droplets. By adjusting the liquid flow rate and the piezoceramic frequency, it is possible to increase the droplet spacing up to about six times the droplet diameter. This, however, is accompanied by a modification of droplet sizes. The droplets are then injected into an enclosure fed with hot air coming from an electrical heater. In order to limit the thermal losses, a resistive electrical wire is inserted within the enclosure wall so that the wall temperature can be regulated to match that of the entering air. A temperature of up to 673 K could be reached. Destabilization of the droplet stream by the air motion can be a critical issue in this experiment. The air velocity is therefore maintained at between 0.1 and 0.3 m/s and the air flow is quietened by forcing it to go through a drilled wall and metallic foam. The problem of vapour saturation must be considered carefully due to the moderate movement of the air and the finite dimension of the chamber which has an inner diameter of 10 cm and a height of 14 cm. An estimate of the diffusion length L_d can be obtained considering diffusivity D_{Fa} is of the order of 10^{-5} m²/s and maximal diffusion duration t is equal to 25 ms. The latter corresponds to the time required for a droplet to be transported through the enclosure. Based on these data we have $L_d = \sqrt{D_{Fa}t} \approx 0.5$ mm which is negligible compared to the inner radius of the enclosure. This ensures non-saturated conditions. Additionally, glass windows have been mounted in the wall to provide optical access. The two-colour laser-induced thermometry [20] is used to characterize the droplet temperature. The method involves the seeding of the liquid fuel with a small quantity of a fluorescent tracer, pyromethene 597-C8. The ratio of the fluorescence intensity detected on two spectral bands is a function of the temperature regardless of laser intensity, time-dependent tracer concentration, and measurement volume [21]. The velocity of the droplets is measured by Laser Doppler Velocimetry using the same laser light source as for the fluorescence excitation. The droplet size reduction is determined using the light scattering in the forward direction, where a stationary interference pattern is created. The measurement of the angular interfringe provides an accurate measurement of the droplet diameter.

Six liquid fuels were tested: acetone, ethanol, 3-pentanone, n-heptane, n-decane and n-dodecane. The approximations for the binary diffusion coefficients for each are given and discussed in Appendix A. Other physical properties of n-heptane and n-dodecane were assumed to be the same as in [12] (most of these properties were approximated using data from [22,23]). The physical properties of n-decane were taken to be the same as in [24], while the properties of acetone, ethanol and 3-pentanone were taken from [17,22,25].

An investigation of a number of droplet streams was performed. The temperature, velocity and diameter of the droplets were measured simultaneously at each measurement point. The periodicity of the droplets in the chain and the steady-state nature of their stream allowed us to convert the droplet distance from the injector into time. In our analysis, we focused on the evolution of droplets' temperatures and radii, starting from the moment when the first droplet was observed near the entrance to the enclosure. By placing a thermocouple at different locations it was established that air temperature T_a did not vary inside the chamber. Hence, it was considered to be constant during each experiment in our modelling. The droplet absolute velocities were approximated as linear functions of time (measured from the moment of injection):

$$v_d = v_1 - v_2 t, \qquad (5)$$

where constants v_1 and v_2 were determined for each experiment, alongside the ratios $Nu_n = Nu/Nu_{iso}$ and $Sh_n = Sh/Sh_{iso}$, describing the effects of interaction between droplets in the stream, where the subscript $_{iso}$ refers to isolated droplets. The error of determination of v_d is comparable with the ambient air velocities up to 0.3 m/s. This justifies our assumption that the absolute droplet velocities, estimated by Eq. (5), are equal to droplet velocities relative to ambient air. These velocities are used for the estimation of the Nusselt and Sherwood numbers for isolated droplets.

The values of the Nusselt and Sherwood numbers were estimated based on simultaneous measurements of droplet sizes and mean temperatures. These measurements allowed us to evaluate heat fluxes responsible for droplet heating and evaporation rates. These rates, alongside the measured time evolution of droplet mean temperatures, were used for the estimate of the convective heat flux, responsible for droplet heating, and mass flux of fuel vapour leaving the droplet. The main difficulty in converting these estimates into the estimates of the Nusselt and Sherwood numbers relates to the fact that the surface droplet temperatures T_s were not directly measured and had to be estimated. This issue is addressed in [15,17], where an iterative approach based on a simplified analysis of the energy balance of evaporation was used. After the droplet surface temperatures were estimated, the values of

the Nusselt and Sherwood numbers were derived from the estimated heat and mass fluxes. Using the values of these numbers for isolated droplets, calculated from the Abramzon and Sirignano [14] model, the values of Nu_n and Sh_n, presented in Table 1, were calculated.

Three experiments were performed with each fuel, except 3-pentanone, for which only two experiments were performed. The values of T_a, distance parameter C (ratio of the distance between droplets and their diameters), initial droplet diameters D_{d0} (measured directly when the first droplets near the entrance to the enclosure were observed), Nu_n, Sh_n, v_1 and v_2 for each experiment are presented in Table 1, alongside boiling and critical temperatures (T_b and T_c) for each substance [22]. The values of C are shown to indicate the closeness of droplets in our experiments. In contrast to [6] they were not used to estimate Nusselt and Sherwood numbers.

The uncertainties in the measurement of the droplet diameters are expected to be about ±0.5 μm in most cases and the uncertainties in the temperature measurements are expected to be about ±1 K. Depending on the fuel and the experimental conditions, the uncertainties in the estimates of Sh_n and Nu_n are expected to be between 2% and 25% [15]. However, in the case of n-decane and n-dodecane, which have particularly low volatility, the mass loss due to evaporation was so low that it was not possible to determine accurately a value for Sh_n. Therefore, for these cases, the values of Sh_n were not estimated experimentally and we assumed them to be equal to Nu_n.

4. Results

The plots of temperature versus time for Case 1 for acetone and n-heptane, calculated using our model and obtained in the experiment are shown in Figs. 1 and 2. The values of parameters shown in Table 1 were used in calculations. The calculations were performed ignoring the interactions between droplets (indicated by subscript $_{iso}$) and taking them into account, based on the values of Sh_n and Nu_n given in Table 1. Time in all figures is measured from the moment of injection.

Table 1
The values of T_a, C, D_{d0}, Nu_n, Sh_n, v_1 and v_2 for three experiments with acetone, ethanol, 3-pentanone, n-heptane, n-decane and n-dodecane droplets (abbreviated as acet, ethan, 3-pen, n-hep, n-dec and n-dod). The droplet velocities in m/s are approximated as $v_d = v_1 - v_2 t$, where t is in ms. In the case of n-decane and n-dodecane, the values of Sh_n were not estimated experimentally, but assumed to be equal to Nu_n.

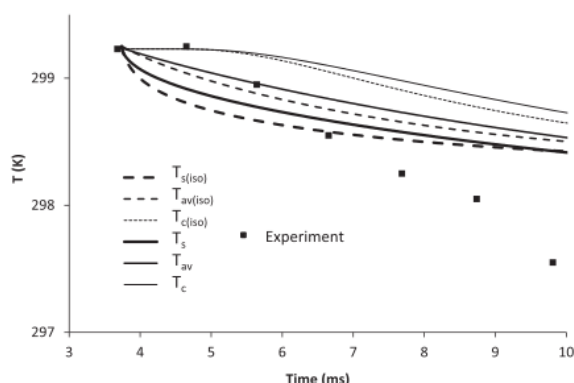| Case	Parameter	Acet	Ethan	3-Pen	n-Hep	n-Dec	n-Dod
	T_b (K)	329.22	351.80	375.14	371.57	477.30	489.48
	T_c (K)	508.10	513.92	561.50	540.20	617.70	658.00
1	T_a (K)	640	643	634	644	643	643
1	C	4.5	4.3	4.9	4.4	3.7	4.6
1	D_{d0} (μm)	122.6	119.6	118.2	131.1	121.5	110.0
1	Nu_n	0.42	0.26	0.23	0.38	0.18	0.19
1	Sh_n	0.43	0.38	0.53	0.57	0.18	0.19
1	v_1 (m/s)	11.16	9.869	10.86	12.8	9.59	9.246
1	v_2 (m/(s·ms))	0.198	0.214	0.254	0.329	0.220	0.281
2	T_a (K)	645	643	645	645	645	644
2	C	5.5	6.1	4.0	5.3	4.4	6.9
2	D_{d0} (μm)	132.2	130.28	123.3	134.2	128.37	129.0
2	Nu_n	0.43	0.42	0.22	0.35	0.24	0.22
2	Sh_n	0.42	0.82	0.33	0.84	0.24	0.22
2	v_1 (m/s)	14.12	12.64	9.454	15.44	11.88	13.14
2	v_2 (m/(s·ms))	0.276	0.268	0.224	0.446	0.329	0.573
3	T_a (K)	647	644	n/a	647	647	643
3	C	3.3	3.1	n/a	3.8	5.4	3.0
3	D_{d0} (μm)	107.2	112.4	n/a	122.8	124.8	98.99
3	Nu_n	0.35	0.36	n/a	0.28	0.18	0.22
3	Sh_n	0.26	0.38	n/a	0.50	0.18	0.22
3	v_1 (m/s)	7.122	6.889	n/a	10.56	13.55	6.091
3	v_2 (m/(s·ms))	0.113	0.123	n/a	0.244	0.307	0.218

Fig. 1. Plots of the time evolution of the experimentally observed temperatures of acetone droplets for Case 1, and temperatures at the surface of these droplets (T_s), average temperatures in the droplets (T_{av}) and the temperatures at the centre of the droplets (T_c), predicted by the models ignoring the interactions between droplets (indicated by the subscript $_{iso}$), and taking into account these interactions. The input parameters of the models were taken from Table 1.
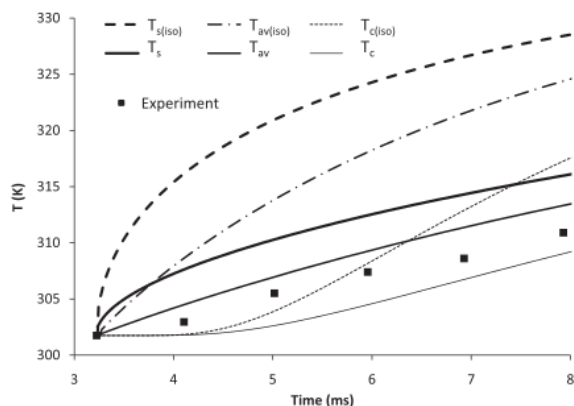

Fig. 2. The same as Fig. 1 but for *n*-heptane droplets.

The calculations started at the time when the droplets were first observed near the entrance to the chamber. The observed temperatures and radii of these droplets were used as the initial temperatures and radii in the model. It was assumed that initially there was no temperature gradient inside droplets.

As follows from Figs. 1 and 2, the plots referring to interacting and non-interacting (isolated) droplets are noticeably different for both substances. Similarly, the plots referring to the temperatures at the centres of the droplets, average temperatures, and the temperatures at the surfaces of the droplets are well separated. This result is similar to the one reported in [6], and it shows the limitation of the assumption, which is widely used in CFD codes, that the gradient of temperature inside droplets can be ignored.

The observed temperatures of acetone droplets, shown in Fig. 1, look rather different from the ones predicted by the model. Note, however, that the difference between the average temperature, predicted by the model, taking into account the interaction between droplets (T_{av}), and the experimentally observed temperatures is always less than 1 K, and can be naturally attributed to the uncertainty of the measurements, and uncertainties of the input parameters used in calculations.

In the case of *n*-heptane and *n*-dodecane droplets, the closeness between the experimentally observed temperatures and T_{av} was

the most visible, compared with other droplets. The best matching between the experimentally observed temperatures and T_{av} can be seen for *n*-heptane, as shown in Fig. 2. However, even in this case, the actual deviation between these temperatures sometimes exceeds 1 K. This means that the model cannot predict the observed average droplet temperatures with errors less than about 1 K. For both these substances, the experimentally observed temperatures always lie between the temperatures T_s and T_c, predicted by the model, taking into account the interaction between droplets.

In the case of ethanol droplets the experimentally observed temperatures were closer to the ones predicted by the model, taking into account the interaction between droplets, than the one ignoring this interaction. However, the deviation between the experimental points and T_{av} for these droplets (up to about 3 K) was larger than in the case of acetone, *n*-heptane and *n*-dodecane droplets. The temperatures for 3-pentanone and *n*-decane were generally similar to those for ethanol, with the maximal deviation between the experimental points and T_{av} about 3 K for 3-pentanone and about 6 K for *n*-decane.

The plots of normalised droplet radii R_d/R_{d0} versus time for Case 1 for all six substances, calculated using our model and obtained in the experiment, are shown in Figs. 3 and 4. The initial values of droplet radii were taken to be equal to those for the droplets for which the first measurements of droplet temperature were taken.

When calculating the time evolution of R_d, both droplet evaporation and thermal expansion were taken into account based on Eq.
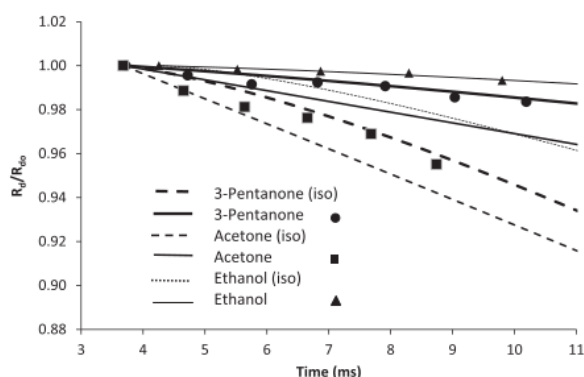

Fig. 3. Plots of the time evolution of the experimentally observed and modelled normalised droplet radii R_d/R_{d0} for acetone, ethanol and 3-pentanone droplets for Case 1. Models ignoring the interactions between droplets (indicated by the subscript $_{iso}$), and taking into account these interactions, were used. The input parameters of the models were taken from Table 1.
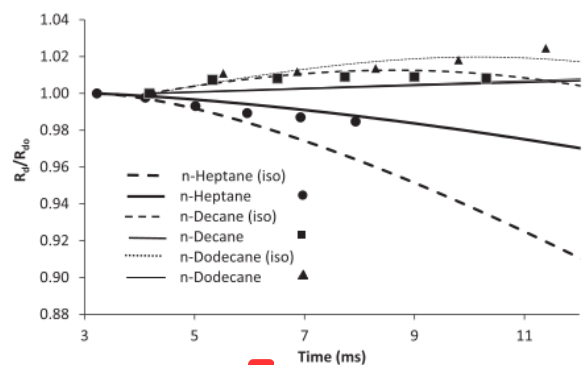

Fig. 4. The same as Fig. 3 but for *n*-heptane, *n*-decane and *n*-dodecane droplets.

(3). The values of parameters used for these calculations are given in Table 1. As follows from these figures, the plots referring to interacting and non-interacting droplets are noticeably different for all substances, as for the temperature plots shown in Figs. 1 and 2. Note that in contrast to [15] we presented the plots of the ratios of radii rather than the ratios of radii squared. The latter would have been justified if the analysis had been focused on droplet evaporation beyond the heat-up period, when the d^2-law is valid. In our case, however, the focus is on the heat-up period itself (cf. [26]).

As follows from Figs. 3 and 4, the effects of interaction between droplets lead to a decrease in the rate of reduction of their radii in the case of acetone, ethanol, 3-pentanone and n-heptane, but to a slowing down of the increase of these radii in the case of n-decane and n-dodecane. In the latter case, the effect of the thermal expansion of droplets dominates over the effects of evaporation. In the case of ethanol, 3-pentanone, n-heptane and n-decane the agreement between experimental plots and predictions of the model, taking into account the interaction between droplets, looks almost ideal. However, for acetone and n-dodecane the experimental data lie between the predictions of the models ignoring the interaction between droplets and taking them into account. Even in the case of these two substances, the deviation between the experimental results and the predictions of the model, taking into account the interaction between droplets, does not exceed about 2%.

For the results referring to Cases 2 and 3 we restricted our analysis to comparison of the experimental data with the average temperatures and R_d/R_{d0} predicted by the model taking into account the interaction between droplets, as was done in [15]. Instead of the actual droplet average temperatures T, studied for Case 1, the analysis for Cases 2 and 3 is focused on the difference between these temperatures and the initial droplet temperatures T_0. The corresponding plots for $T - T_0$ versus time for Case 2 for all six substances are shown in Fig. 5. As follows from this figure, although the trends predicted by the model are similar to the ones observed experimentally, there are noticeable deviations between the actual values of predicted and observed average droplet temperatures. The maximal deviation between them is seen for n-decane and n-dodecane droplets. The minimal deviation between them is seen for 3-pentanone droplets.

The plots of R_d/R_{d0} versus time for Case 2 for the same substances as in Fig. 5, are shown in Fig. 6. As one can see from this figure, the trends predicted by the model are similar to the ones
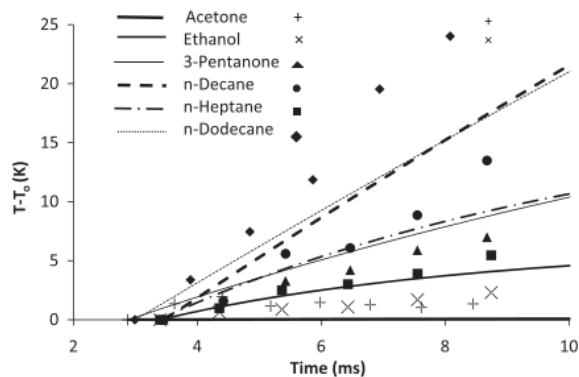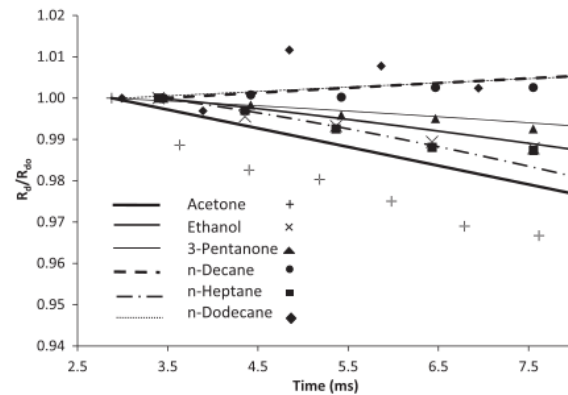

Fig. 6. The same as Fig. 5 but for R_d/R_{d0}.

observed experimentally, but there are noticeable deviations between the observed and predicted values of this ratio, as in the case of Fig. 5. The maximal deviation between these ratios (up to almost 2%) is seen for acetone droplets. The minimal deviation between these ratios is seen for 3-pentanone droplets. Hence, for Case 2 the best agreement between experimental and modelled results for both temperatures and radii is observed for 3-pentanone droplets.

The plots for $T - T_0$ versus time for Case 3 for acetone, ethanol, n-heptane, n-decane and n-dodecane (there is no data for 3-pentanone for Case 3) are shown in Fig. 7. As one can see from this figure, the agreement between experimental and modelled results is very good for acetone, while the deviation between the experimentally observed temperatures and those predicted by the model could reach more than about 5 K for ethanol and n-dodecane (although the observed and predicted trends for both substances are the same). The plots of R_d/R_{d0} versus time for Case 3 for the same substances as in Fig. 7, are shown in Fig. 8. As can be seen from this figure, the best agreement between experimental and modelled results can be seen for n-decane and n-heptane, and the worst for acetone and n-dodecane. However, even in the case of acetone and n-dodecane, both experimental and modelled results show the same trends and the deviation between them does not exceed 2%.

Several factors are expected to contribute to the difference between the modelled results presented in this paper and ones reported in [15,17]. Some approximations for transport coefficients used in this paper are different from those used in [15,17]. We used the time-averaged values of Nu_n and Sh_n, while both these parameters varied with time.
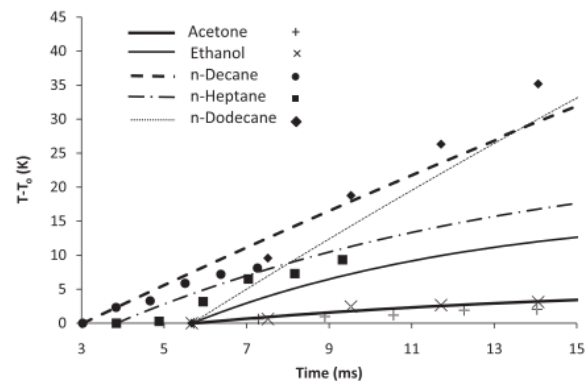

Fig. 5. Plots of the time evolution of the experimentally observed droplet temperatures $T - T_0$, where T_0 are the initial droplet temperatures, and the average temperatures of droplets, predicted by the model taking into account the interaction between droplets. The results for acetone, ethanol, 3-pentanone, n-heptane, n-decane and n-dodecane droplets for Case 2 are shown. The input parameters of the models were taken from Table 1.

Fig. 7. The same as Fig. 5 but for Case 3, except without the results for n-pentanone.
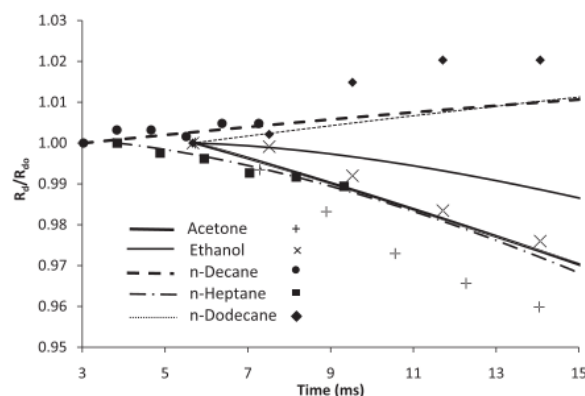
Fig. 8. The same as Fig. 7 but for R_d/R_{d0}.

5. Conclusions

Heating and evaporation of monodisperse acetone, ethanol, 3-pentanone, n-heptane, n-decane and n-dodecane droplets in ambient air at fixed temperature and atmospheric pressure have been studied numerically and experimentally. Droplet initial diameters varied from 99 to 135 μm, while ambient air temperatures varied from 634 to 647 K. The numerical model took into account the finite thermal conductivity of droplets and recirculation inside them based on the effective thermal conductivity model and the analytical solution to the heat conduction equation inside droplets. The initial values of droplet temperatures and radii were assumed to be equal to those observed experimentally for the first recorded droplet. It was assumed that initially there was no temperature gradient inside droplets.

It is pointed out that the interactions between droplets lead to noticeable reduction of their heating in the case of ethanol, 3-pentanone, n-heptane, n-decane and n-dodecane droplets, and enhancement of their cooling in the case of acetone. The interaction between droplets leads to a decrease in the rate of reduction of their radii in the case of acetone, ethanol, 3-pentanone and n-heptane, but to a slowing down of the increase of these radii in the case of n-decane and n-dodecane. In the latter case, the effect of the thermal expansion of droplets dominates over the effects of evaporation.

Although the trends of experimentally observed droplet temperatures and radii are the same as predicted by the model taking into account the interaction between droplets, the values of the predicted droplet temperatures can differ from the observed ones by up to about 8 K, and the actual values of the predicted droplet radii can differ from the observed ones by up to about 2%.

Combining the above results and those reported previously in [6] we can conclude that the effective thermal conductivity model, based on the analytical solution to the heat conduction equation inside droplets, can predict the observed average temperature of droplets with possible errors not exceeding several K, and observed droplet radii with possible errors not exceeding 2% in most cases. These results confirm our previous conclusion (see [9,10,12]) that this model can be recommended for implementation in CFD codes and used for multidimensional modelling of spray heating and evaporation based on these codes.

Acknowledgements

Appendix A. Binary diffusion coefficient for fuel vapour

The binary diffusion coefficient for all fuels was estimated using the following equation [27]:

$$D_{Fa} = 1.8583 \times 10^{-7} \sqrt{T^3 \left(\frac{1}{M_F} + \frac{1}{M_a} \right)} \frac{1}{p \sigma_{Fa}^2 \Omega_{Fa}(T^*)}, \qquad (A1)$$

where D_{Fa} is in m²/s, p is in atm (1 atm = 0.101 MPa), T is in K, $\sigma_{Fa} = 0.5(\sigma_F + \sigma_a)$ is the minimal distance between molecules in Angström, Ω_{Fa} is the collision integral, the value of which depends on the normalised temperature $T^* = Tk_B/\epsilon$, k_B is the Boltzmann constant, $\epsilon = \sqrt{\epsilon_F \epsilon_a}$; the subscript $_a$ indicates air. Note that the formula for the binary diffusion coefficient used in [22] differs from the one presented above in terms of the value of the coefficient (they used 1.8623 instead of 1.8583). The difference between the values of this coefficient predicted by two formulae (0.2%) can be safely ignored in most practical applications. Note that there is a typo in Eq. (B5) of [12]. $\sigma_a = 3.617$ Angström, $\epsilon_a/k_B = 97.0$ K (Table E.1 in [27]). The values of these parameters and molar masses for acetone, ethanol, n-heptane, 3-pentanone and n-dodecane are given in Table A1.

There is some controversy regarding the values of σ_F and ϵ_F/k_B for n-heptane and n-dodecane. We used the data leading to the best fit with experimental data. These are indicated by * in the ϵ_F/k_B column.

Once the value of T^* had been found, the collision integral Ω_{Fa} could be obtained from Table E.2 [27]. However, we found it more convenient to use the analytical approximation of Ω_{Fa} given by Eq. (E.2-2) of [27]).

For the binary diffusion coefficient of n-decane ($C_{10}H_{22}$) we used the following approximation [24]:

$$D_{Fa} = 5.46 \times 10^{-6} \frac{1}{1.01\,p} \left(\frac{T}{300} \right), \qquad (A2)$$

where p is in atm, as in Eq. (A1).

Table A1
The values of σ_F, ϵ_F/k_B and molar masses for acetone, ethanol, n-heptane, 3-pentanone and n-dodecane, as inferred from various sources.

Fuel	Reference	Formula	σ_F in Angström	ϵ_F/k_B in K	Molar mass in kg/kmole
Acetone	[22]	C_3H_6O	4.600	560.2	58.080
Ethanol	[22]	C_2H_6O	4.530	362.6	46.069
n-Heptane	[28,22]	C_7H_{16}	5.949	399.3*	100.204
n-Heptane	[27]	C_7H_{16}	6.663	352	100.20
n-Heptane	[29,22]	C_7H_{16}	6.498	455.04	46.069
3-Pentanone	[28,22]	$C_5H_{10}O$	4.22	351.562	86.134
n-Dodecane	[28,22]	$C_{12}H_{26}$	9.37	245.0	170.338
n-Dodecane	[29,22]	$C_{12}H_{26}$	6.5972	454.6768*	170.338

Data indicated by * in the ϵ_F/k_B column were used in our analysis.

Monodisperse monocomponent fuel droplet heating and evaporation